DISCLAIMER NOTICE

THIS DOCUMENT IS THE BEST QUALITY AVAILABLE.

COPY FURNISHED CONTAINED A SIGNIFICANT NUMBER OF PAGES WHICH DO NOT REPRODUCE LEGIBLY.

High-Power Tube Program

Semiannual Technical Summary Report
to the
Advanced Research Projects Agency

31 December 1961

Lincoln Laboratory
Massachusetts Institute of Technology

MASSACHUSETTS INSTITUTE OF TECHNOLOGY

LINCOLN LABORATORY

HIGH-POWER TUBE PROGRAM
SEMIANNUAL TECHNICAL SUMMARY REPORT
TO THE
ADVANCED RESEARCH PROJECTS AGENCY

31 DECEMBER 1961

ISSUED 22 JANUARY 1962

The work reported in this document was performed at Lincoln Laboratory, a center for research operated by Massachusetts Institute of Technology; this work was supported by the U.S. Advanced Research Projects Agency, Order No. 85, under Air Force Contract AF 19(604)-7400.

LEXINGTON MASSACHUSETTS

TABLE OF CONTENTS

I. INTRODUCTION

The high-power tube program was established to investigate some of the basic problems encountered in amplifiers now under development or planned for future radar and communications use.

During the period covered by this report, work on vacuum voltage breakdown was reinitiated. Emphasis is being placed on breakdown across ceramic insulators because of the difficulty that has recently been experienced with this phenomenon.

A study of grid configurations having possible application to switch tubes or linear beam tubes has been started. Interest is centered on grids that are elongated in the direction of electron flow, since it is felt that this type of grid may be useful in applications where wire grids fail because of their low-power dissipation capability. This work is motivated by radar requirements for short pulses and asynchronous pulsing modes.

Measurements with the beam-impulse heating tube indicate that significant damage occurs to a copper surface with peak-power densities of approximately 0.5 Mw/cm^2 in a few seconds' operation at a duty cycle of 0.003 (10-μsec pulses). Calibration of the temperature-measuring equipment has been the most difficult part of this project.

Theoretical predictions of TR tube performance, made with the 7090 computer, have been verified by measurements on an L-band folded-cylinder TR tube. Construction of the S-band ring resonator has been completed. This unit, when installed, should permit testing of S-band components at simulated average powers of 500 kw.

The biased-collector tube has been placed in operation and measurements have been started. Work to date has been at relatively low-voltage levels.

Details of the foregoing projects, as well as of cathodes, vacuum techniques, klystron analysis and cavity-loss distribution are described on the following pages.

Work on hollow beams at Varian Associates is not described in this semi-annual report since the experimental portion of that contract has been completed and no new data have been obtained during this period. A final report is in preparation.

The secondary-emission work has been completed and a report written. No further investigations are planned at this time, with the exception of an experiment to determine the efficacy of some of the coatings in inhibiting multipactor in a resonant cavity.

R. C. Butman

II. KLYSTRON ANALYSIS AND EXPERIMENT

During the course of efforts to formalize the space-charge-wave linear analysis, it was discovered the energy conservation condition (kinetic power theorem) was not fulfilled. The omission was finally determined to be the term corresponding to the electromagnetic energy of the bunched beam current in the tunnel following the gap. The energy conservation theorem, including this electromagnetic energy, could then be satisfied. Although the magnitude of this term was about 15 per cent, its net contribution to the electronic gap conductance was negligible (2 per cent maximum in the case of a perveance 10 hollow beam) and so need not be included in the calculation of Q_{e1} for ordinary klystron beams. The electromagnetic energy contribution has been the concern of R. L. Pease.*

There has been little opportunity since the last semiannual report to obtain additional gain or phase vs frequency data. However, the following items have received some attention:

(a) The instrumentation for phase measurement has been improved in sensitivity to something better than ±1°. Normal variation in tube operating conditions, line voltage, temperature, tuning, etc., are limiting the reproducibility of measurements.

(b) The correction mentioned in the last semiannual report[1] to the stagger tuned amplitude response due to the frequency sensitivity of the nontunable portion of the output circuit has been made with the result shown in Fig. II-1. It is evident that this helps to bring the computed shape toward better agreement with the experimental response. Most of the remaining disagreement may be the result of a higher effective Q_{e1} for the intermediate cavities than results from the calculation. This (too low calculated Q_{e1}) in turn may be a fault in the theory or a poor estimate of the beam size used in the calculation.

---

* Consultant

(c) A single run has been made on a VA 87 klystron of relative phase vs amplitude of RF drive which indicates that phase excursions of a few tens of degrees occur in the large-signal region. The dependence on amplitude of this variation appears to follow what one would expect from the manner in which the phase of the RF output voltage is determined with respect to the bunched beam. A quantitative comparison will be made as soon as additional data can be taken to confirm this preliminary run and an analysis is formulated to compute the theoretical behavior.

G. L. Guernsey

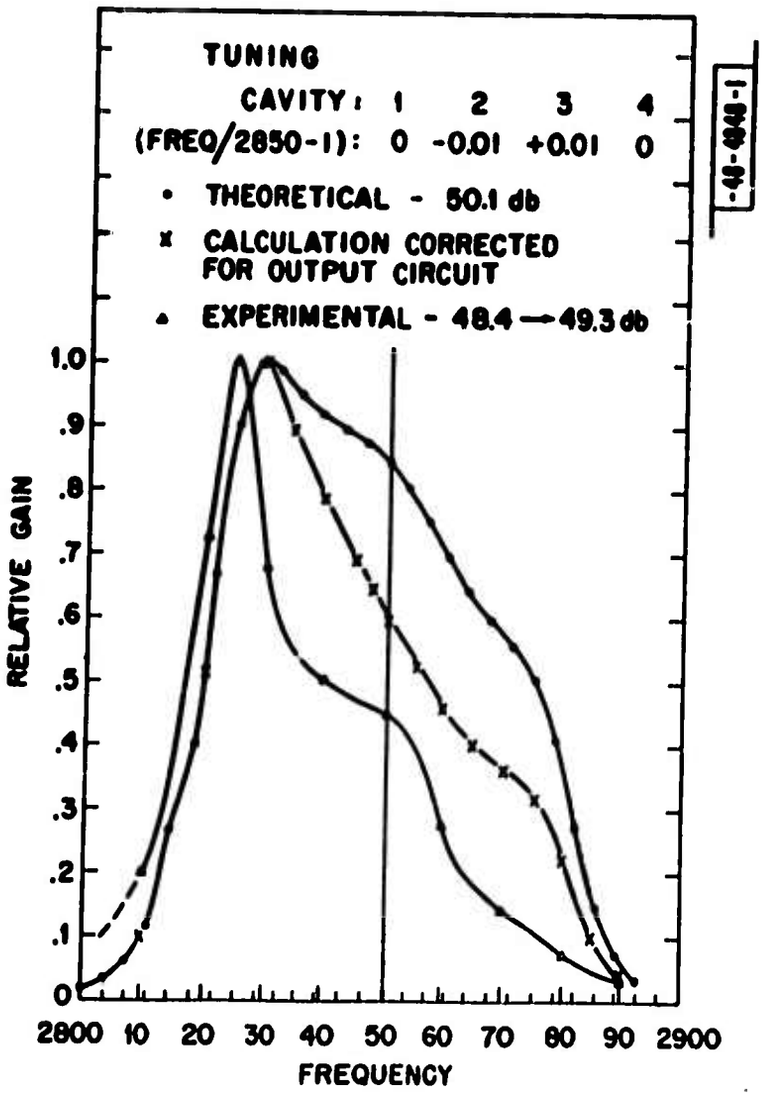

Fig. II-1. Klystron gain vs frequency (VA 87C).

III. BEAM PULSE HEATING

The purpose of this project is to measure the intrapulse heating and evaporation rates of metallic surfaces bombarded by high-intensity pulsed electron beams.

The second beam pulse heating tube (XT455, Ser. 2) was fabricated, processed and pulsed during this reporting period. Four OFHC copper targets were installed with the first target (No. 21) used primarily to study cathode emission and beam formation. A considerable amount of time was spent adjusting the magnetic field to obtain uniform density over the beam at the target. A magnetic field of about 250 gauss was required to obtain the 0.6-inch-diameter beam that was finally used.

During the investigation of the electron beam, the inside glass surface of the tube became coated with vaporized copper. For this reason, temperature measurements with the photoelectric pyrometer could not be made on the remaining three targets. These three were then used in an effort to measure the rate of evaporation of OFHC copper under conditions simulating those existing in a tube now under development. The remaining three targets (22, 23, 24) were therefore pulsed at 28 kv, 10-μsec pulse duration, 0.55-Mw/cm^2 peak beam power density, 300-pulse-per-second (pps) repetition frequency with 101 pulses bombarding target 24, 1010 pulses on target 23 and 10,004 pulses on target 22.

Photographs of the four targets after bombardment are shown in Figs. III-1(a) through (d). Figure III-1(a) shows the test copper target 21. The total number of pulses impinging on this target was 11,969 at peak voltages that ranged from 20 kv to 86 kv. A crater $\frac{1}{16}$-inch diameter by $\frac{1}{16}$-inch deep is easily identified on the photograph. It is worth noting that a spot approximately $\frac{1}{16}$-inch diameter was initially discernible optically as a result of 21 pulses at 38-kv peak voltage.

Figure III-1(b) is a photograph of target 22 bombarded with 10,004 pulses. Here one clearly sees the effect of 33 seconds of 28-kv pulse bombardment on a copper surface at a 300-pps repetition frequency. The spot diameter is approximately $\frac{1}{4}$ inch. Physical damage to the surface is apparent from this

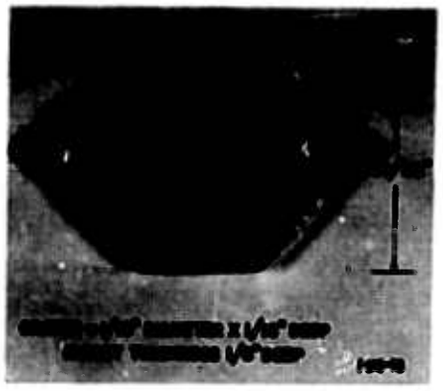

(a) Target 21 (total number of pulses = 11,968).

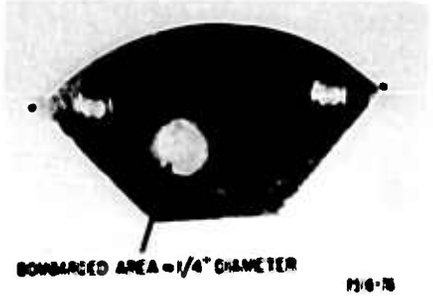

(b) Target 22 (total number of pulses = 10,004).

(c) Target 23 (total number of pulses = 1010).

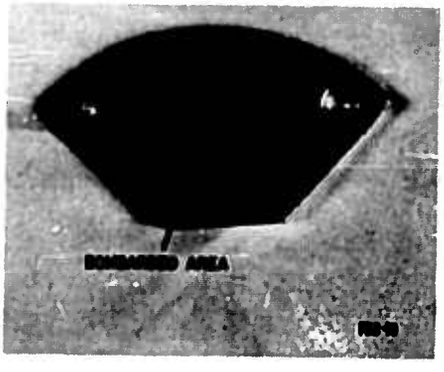

(d) Target 24 (total number of pulses = 101).

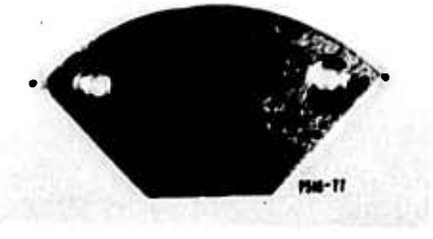

Fig. III-1. Four targets after bombardment with XT455, Ser.2.

photograph. Fissures along the grain boundary which result from the localized heating vary in depth from 6 to 52 microns. Figure III-2(a) is a microphotograph of target 22 before bombardment, showing the grain structure under 50X magnification. Figure III-2(b) is a microphotograph of the same target after bombardment.

Figure III-1(c) is a photograph of target 23 bombarded with 1010 pulses. The area of pulse heating is again easily discernible on the photograph. The spot diameter is approximately $\frac{1}{4}$ inch. Physical damage to this surface is apparent after 3 seconds of pulsed bombardment at a 300-pps repetition frequency.

Figure III-1(d) is a photograph of target 24 bombarded with 101 pulses. No visible signs of damage or localized heating are observed.

During pulse operation of the tube, peak currents impinging on the target pass through the two stainless steel screws that hold the target to the copper backing plate. Heating at these two screws caused the copper targets to be fused to the copper backing plate at the screw hole opening. When the four targets were forcibly removed from this plate for weighing, some of the target copper ripped away, resulting in an increased loss of target weight over that due to electron bombardment. Therefore, no quantitative measurement of target weight loss is reported.

A second set of four copper targets was installed in XT455, Ser. 2, and the tube was reprocessed with a new cathode assembly. It was planned that this second tube would be used in an attempt to obtain quantitative data on temperature rise and additional data on surface evaporation rates.

Since there had been some question about the uniformity of beam density in the first tube, pictures were taken of the target spot at various magnetic fields with anode voltages from 28 to 75 kv. Figure III-3 shows the test setup used; Figs. III-4 through III-7 are typical pictures taken of the spot. It is evident that the beam density is not uniform [Fig. III-5(a)] and further that the target spot is at least partially obscured by a plasma discharge [Figs. III-4(b), 5(b), 6(b), 7(b-c)] at the higher beam power densities. A quantitative determination of the equivalent power density, therefore, requires a more precise determination of the effective beam cross section than has been done to date.

Fig. III-2. Microphotographs of target 22: (a) before bombardment.

Fig. III-2. Microphotographs of target 22: (b) after bombardment with 10,004 pulses.

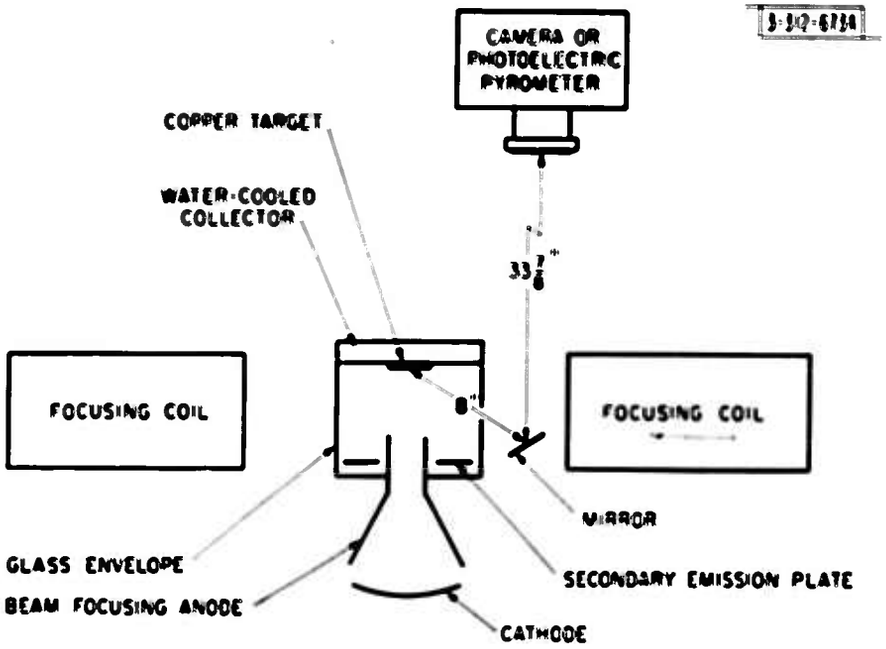

Fig. III-3. Experimental setup for observing bombarded area.

-312-6735(a-b)

(a) 240 gauss. (b) 260 gauss.

Fig. III-4. Bombarded area at 51.5 kv peak voltage.

-312-6736(a-b)

(a) 240 gauss. (b) 260 gauss.

Fig. III-5. Bombarded area at 58 kv.

-312-6737(a-b)

(a) 240 gauss. (b) 260 gauss.

Fig. III-6. Bombarded area at 62 kv.

-312-6738(a-c)

(a) 240 gauss. (b) 260 gauss.

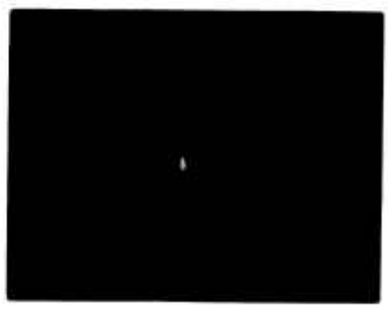

(c) 280 gauss.

Fig. III-7. Bombarded area at 75 kv.

When a qualitative picture of the beam density profile had been obtained, attention was directed toward the problems of measuring the intrapulse temperature as a function of peak voltage and beam power density. Temperature spectrum measurements were also made with the aid of optical long-pass filters whose cutoff wavelengths and transmission characteristics are accurately known. These experiments have shown that the temperature results reported in the last Semiannual Technical Summary Report are incorrect, since the fluorescence and emission spectra of the bombarded copper target do contribute appreciably to the over-all light output spectrum from the bombarded surface. To filter out these unwanted spectra, long-pass filters with cutoff wavelengths 0.52μ, 0.54μ, 0.65μ and 0.7μ were inserted in front of the 7102 photomultiplier tube. Results at 58 kv are shown in Fig. III-8. In this figure, the amplitude of the output pulse from the 7102 photomultiplier tube is plotted against the filter inserted for that measurement. Curve A was taken at 58 kv with a focusing field of 210 gauss. Curve B was taken at the same voltage, but with zero magnetic field with resultant larger beam diameter and lower-power density. One can see that the visible light contribution is essentially removed by the 0.57-μ filter in both cases and that there is a significant thermal contribution showing in the case of high beam density (curve A) in the 0.65- to 0.7-μ region, as evidenced by the decreasing amplitude of response in the low-frequency region.

A typical temperature pulse measured with a 0.7-μ filter inserted is shown in Fig. III-9 for a peak voltage of 67 kv. Both the temperature and corresponding collector current pulse are shown in Fig. III-9(a). The time scale is 5 μsec/cm and the peak amplitude of the current pulse is 25 amp. In Fig. III-9(b) the leading edges of both pulses are shown (time scale is 1.0 μsec/cm). The small step on the leading edge of the temperature pulse is a transient induced by the modulator pulse and does not represent a temperature change. The temperature threshold is believed to be about 760°K. The flat top of the pulse is believed to occur at 1350°K, the melting point of the copper. The temperature rise is therefore about 330°C/μsec. Using an approximate figure for beam diameter of 0.6 inch, the peak power density reached in Fig. III-9 is

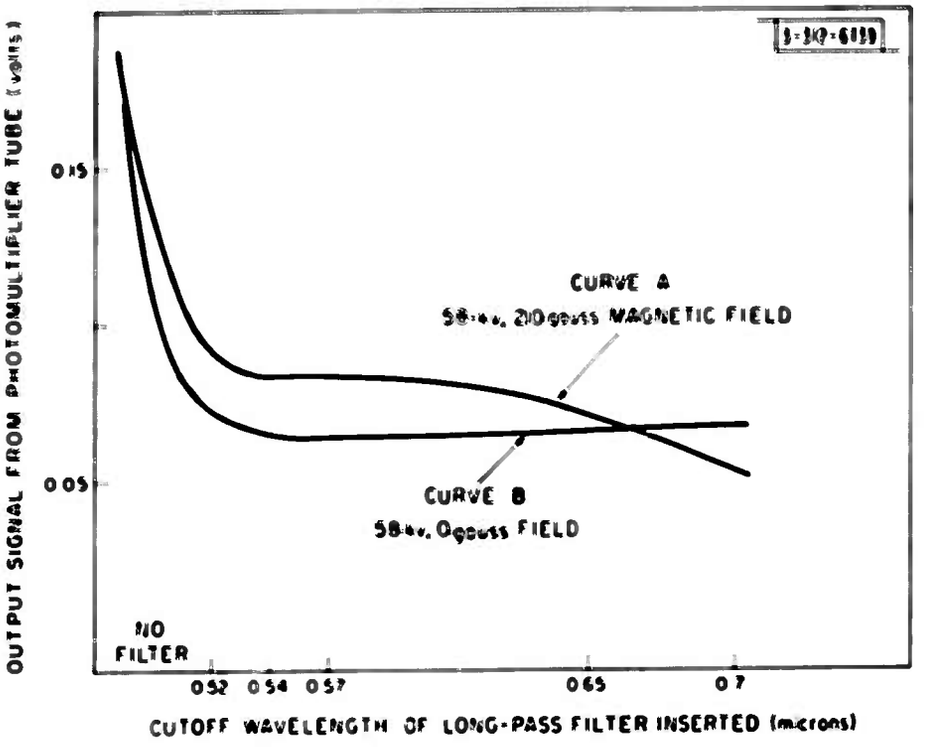

Fig. III-8. Temperature-pulse amplitude vs low-pass filter.

-312-6740

Temperature

(a)

Peak collector current, 25 amp
(5-μsec/cm horizontal scale)

Leading edge temperature

(b)

Leading edge collector current
(1-μsec/cm horizontal scale)

Fig. III-9. Temperature pulse at 67 kv.

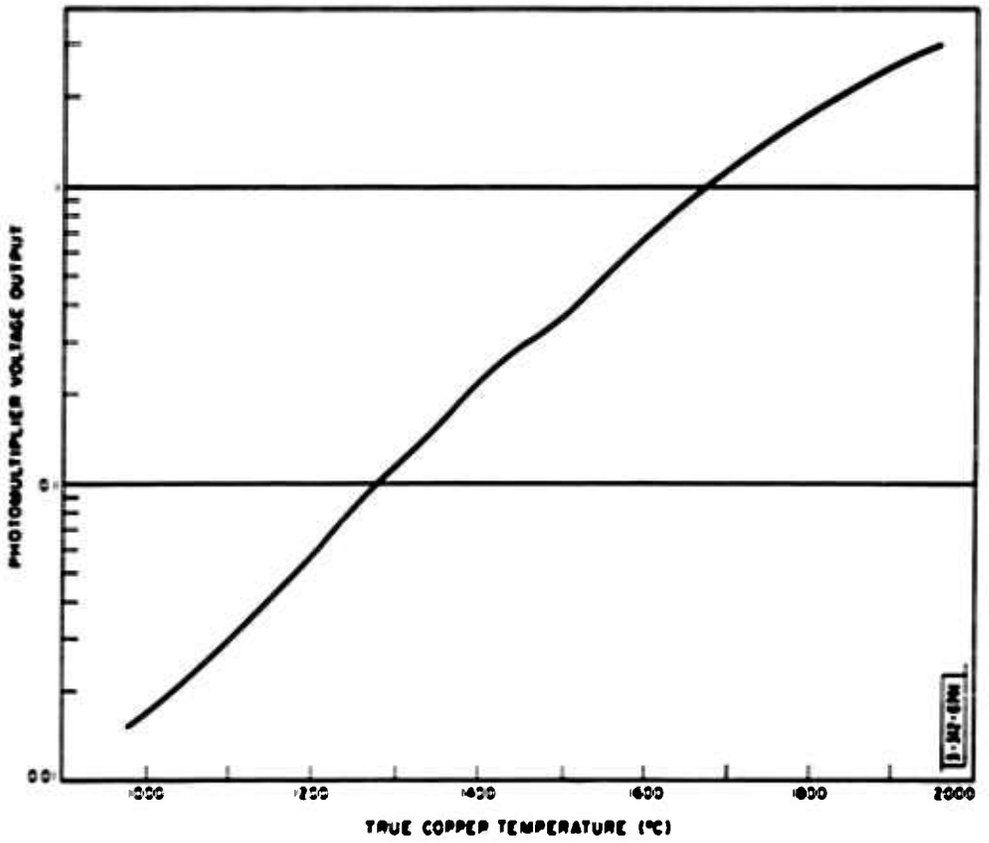

Fig. III-10. Photoelectric pyrometer voltage output vs true copper temperature.

$$\frac{67{,}000 \times 25}{1.82\,\text{cm}^2} = 0.92\,\text{Mw/cm}^2 \quad .$$

The leveling off of the temperature pulse probably results from the fact that the heat of fusion which must be supplied to the copper to cause melting is high enough to prevent a further rise in temperature above the melting point.

Some information on calibration techniques and calculations of temperature rise are offered in support of the foregoing speculation. Consider first the calibration technique. The photocell output current across a load resistor is measured as a function of the temperature of a tungsten source. The light from the source is filtered by a 0.7-μ long-pass filter and interrupted by a flying slot whose area is $0.1\,\text{cm}^2$. The voltage output as a function of temperature, corrected for the difference in emissivity between tungsten and copper is plotted in Fig. III-10. The minimum detectable temperature is about 800°C, or about 1100°K.

With this calibration curve, one can estimate the minimum temperature that can be detected in the actual tube. Since the beam area in the actual beam tube is $1.8\,\text{cm}^2$, one expects that, for identical temperatures of calibrating source and target, the photocell output voltage in the beam tube would be 1.8/0.1 = 18 times that observed with the calibrating source, that is, just the ratio of beam area to calibrating source area. (The field of view of the photocell is large compared with the spot size.) However, from the figure it is found that the photocell voltage varies as (temperature) 7.6. Therefore, the minimum detectable temperature in the tube (taking some liberties with extrapolation techniques) should be

$$\frac{1100^\circ\text{K}}{(18)^{\frac{1}{7.6}}} = 760^\circ\text{K} \quad .$$

The rate of rise of temperature that may be expected can be estimated from a knowledge of the beam power density, the physical constants of the copper target and the range energy relation for electrons in copper.

Consider first Fig. III-11: an approximate plot of the energy density in a copper target as a function of beam voltage, using measured values for beam

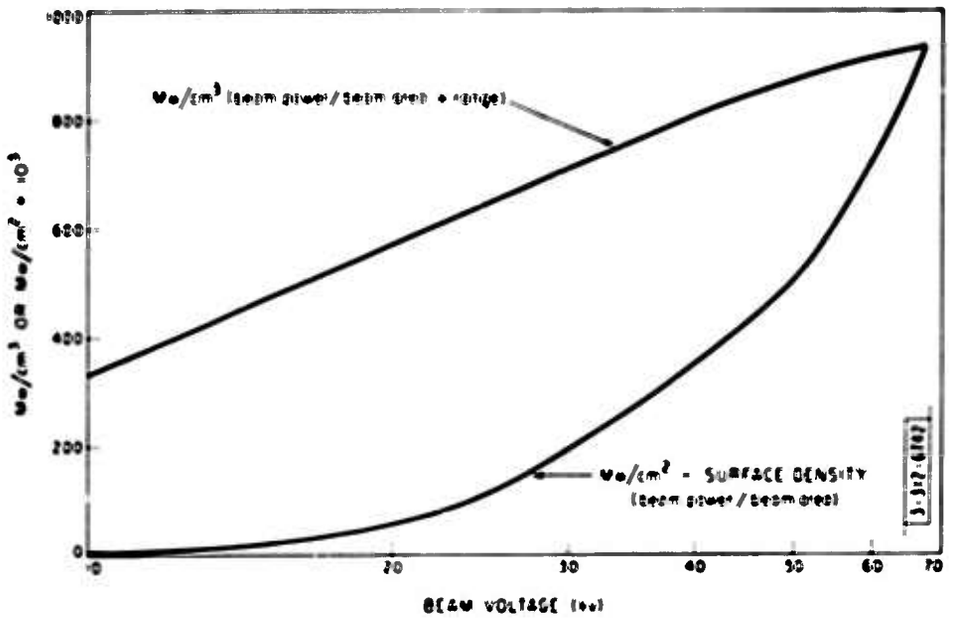

Fig. III-11. Energy densities at bombarded copper surface vs accelerating voltage (beam power = 1.6×10^{-6}, beam area assumed to be 1.8 cm^2 at all power levels).

diameter of 1.5 cm, and beam perveance of 1.6×10^{-6}. The energy density is the average density dissipated in a volume defined by the area of the beam and a depth equal to the practical range for electrons in copper. The principal observation to be made is that the energy density, and therefore the surface temperature, is a slow function of beam voltage. Therefore, one probably does not err greatly by using an average value of energy density when calculating rate of temperature rise at the leading edge of the pulse.

Let us now calculate this rate of rise by using an energy density of 600 Mw/cm^3. The heat capacity of copper is 0.1 cal/gm/°C or 0.418 joule/gm/°C. A power of 600 Mw/cm^3 corresponds to 600 joules/cm^3/μsec or 67.5 joules/gram/μsec. The rate of heating is therefore 67.5/0.418 ≈ 160°/μsec. This corresponds to a 230°/μsec rate estimated by making the assumption that the flat top of the temperature pulse did indeed represent the melting point of copper. Better agreement could hardly be expected in view of the difficulty of beam diameter measurement, and the method used to estimate threshold temperature.

It has been stated that the flat top of the temperature pulse is at 1080°C. The energy required to supply the necessary heat of fusion to melt the copper being bombarded is so large that a limiting action takes place at the melting point. The heat of fusion of copper is 200 joules/gm or 1600 joules/cm^3. Using an energy density of 600 Mw/cm^3, one observes that 2.6μsec (1600/600) would be required to melt copper without raising its temperature when subjected to a bombardment at this level, assuming adiabatic heating. It is a coincidence that the thermal time constants of the copper in this case are of the order of 3μsec, so that one cannot expect the assumption of adiabatic heating to hold beyond (or even to) that length of time. Therefore, with the power densities involved in the experiment reported here, one can expect the temperature to remain at or near the melting point for much longer than 3.0μsec, since there will be appreciable heat flow out of the copper during a period of 3μsec. Indeed, this is the observed fact; the apparent temperature does remain nearly constant for the entire pulse.

E. Silverman

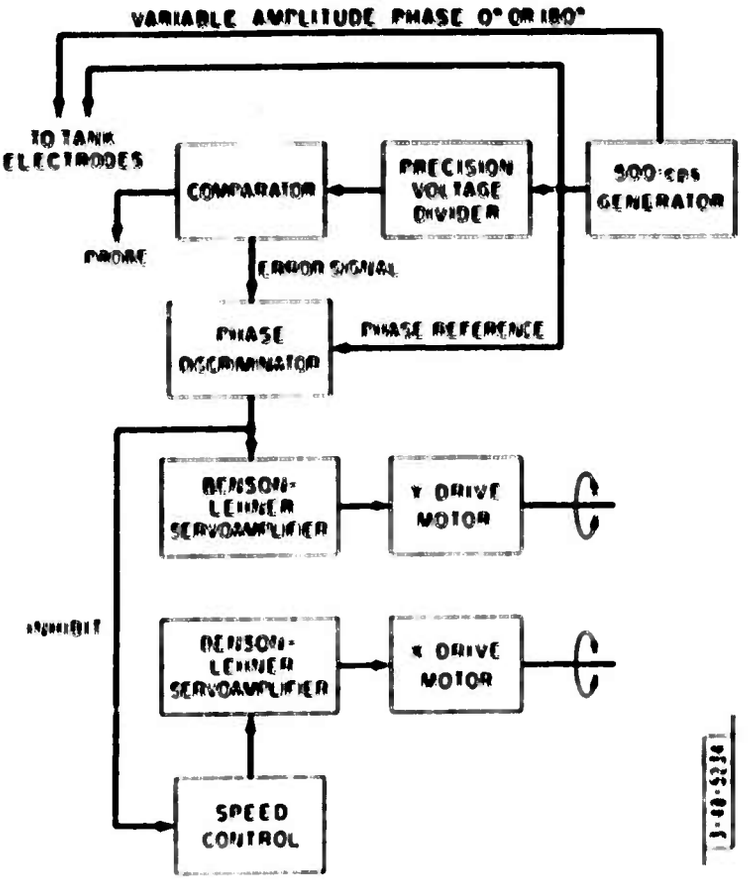

Fig. IV-1. Block diagram for equipotential plotting.

IV. BEAM STUDIES

The construction of the electrolytic tank to be used for high-power electron beam design studies has been completed. The circuits for both potential and electron trajectory plotting are available. The triple probes necessary for trajectory plotting have not yet been received, so that work has thus far been confined to potential plotting.

A block diagram of the circuit used for equipotential plotting is shown in Fig. IV-1. The electrolytic tank and its electrodes are operated with a 500-cps voltage source. This voltage source is divided into 19 equal parts by a precision voltage divider so that 18 equipotential lines can be plotted. The comparator receives one signal from this voltage divider and an input from the electrolyte by way of a probe. A zero output occurs when equality of amplitude is achieved. Inequality is evidenced by a 500-cps signal which is in phase or 180° out of phase with the reference. This signal is converted in the phase discriminator to a DC voltage whose amplitude and polarity is proportional to the amplitude and phase of the error signal with respect to the reference signal. The Benson-Lehner servoamplifier accepts this DC voltage and energizes a 2-phase motor in accordance with this input, causing the probe pickup to move in a direction to reduce the error to zero. Motion in this direction is referred to as the Y direction.

The X motion is produced by inserting a constant DC voltage to the X servo. This drive voltage is reduced by an inhibit signal which is proportional to the magnitude of the error voltage. Thus the X motion may be brought to a halt when an excessive error in Y exists.

A determination of the accuracy and reproducibility of equipotential lines has shown the maximum error to be less than 0.5 per cent and the results to be reproducible within 0.1 per cent. The investigation of accuracy was made by using parallel electrodes. The percentage accuracy is defined as one hundred times the ratio of the difference between the plotted and the calculated position of any line to the total distance between the electrodes. Since the maximum 0.5 per cent error is approximately the same as the maximum error

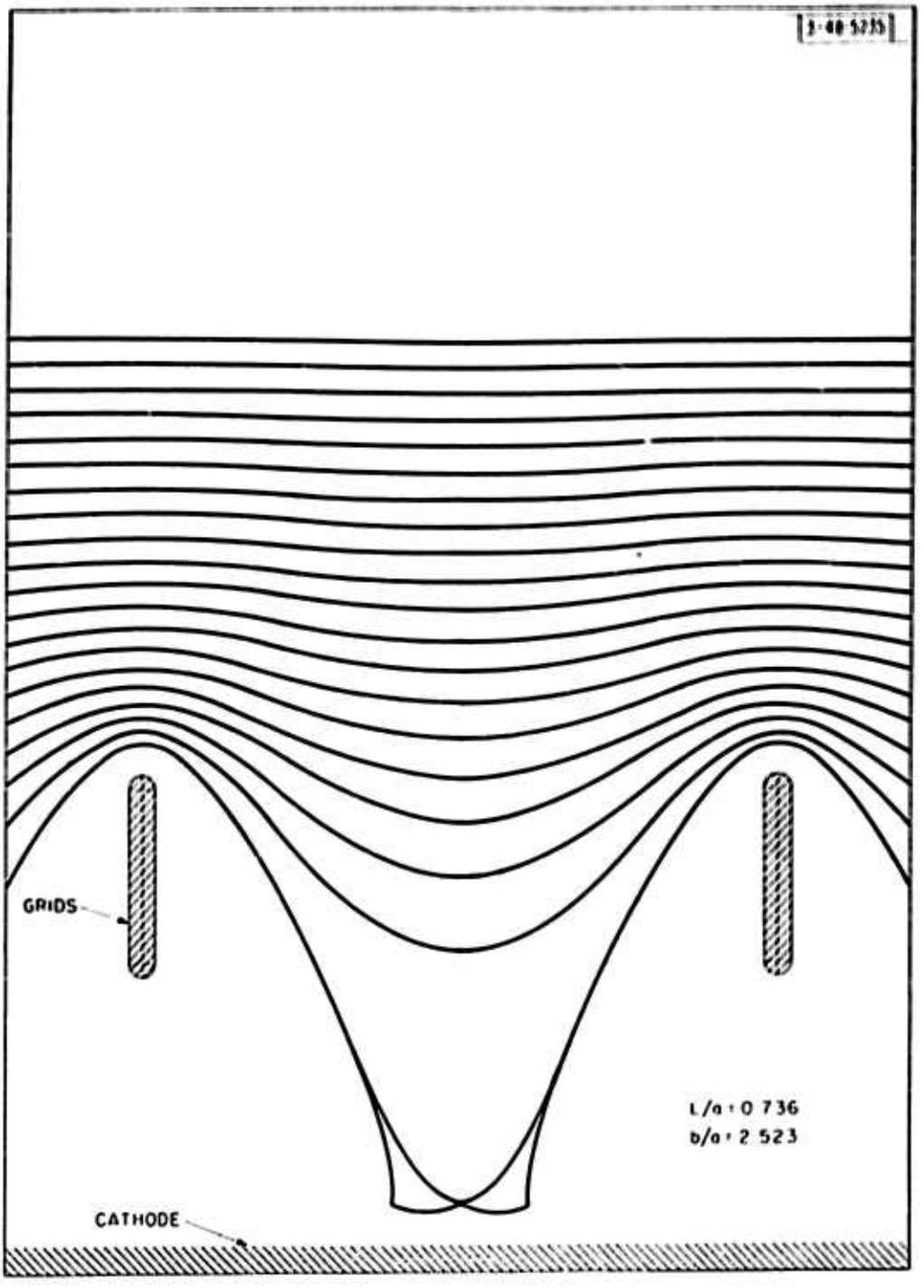

Fig. IV-2. Electrolytic tank equipotential plot.

of the individual resistors used in the voltage divider, it has been decided to rebuild the voltage divider, using resistors with a tolerance of 0.05 per cent in the hope of reducing the error still further. It should be noted here that, even with the degree of accuracy now attained, a considerable error in plotting equipotentials is possible when the gradient, and therefore the error signal, is very small, since the inhibit signal to the otherwise constant drive X servo will be small. It may be seen, for example, in Fig. IV-2, that there was considerable overshoot in the "valley" between grids near the cathode.

To improve the accuracy of the equipment to the 0.5 per cent level, it was found necessary to make mechanical changes in two of the components described in the last High-Power Tube Semiannual Technical Summary Report to ARPA.

The pantograph, which was designed for us to plot the excursion of the probe through the electrolyte, did not have sufficient resistance to bending. Distorted plots were caused by bending and vibration of the pantograph arms. By using commercially available rectangular stainless steel tubing (0.9 in. × 0.4 in. × 0.015 wall for the shorter arms, and 1.872 in. × 0.872 in. × 0.015 wall for the longer arms), it was possible to design a pantograph, each of whose arms offered a minimum of four times the resistance to bending (ten times for the longer arms) for the same weight as the square aluminum tubing (1/2 in. square by 1/16 wall) originally used. The resulting system is far more rigid and therefore able to reproduce more faithfully the probe motion.

The plastic-coated aluminum tilting plane has been replaced by a plexiglass plane. Contrary to expectations, the aluminum plate warped, causing variations in the depth of electrolyte, and thus leading to distortions of the potential lines. Apparently, there was also some capacitive loading of the electrolyte because of a too thin plastic coating on the plate. Finally, it was not possible to mount models easily to this plane, whereas with plexiglass, holes may be easily drilled and models mounted securely. The deformation of the plexiglass plane is to be eliminated by the use of a supporting layer of 3-inch-thick stiff nonabsorbing foam material. This liner will have approximately the same dielectric constant as air and will thus offer the added advantage of more complete isolation from the grounded tank frame.

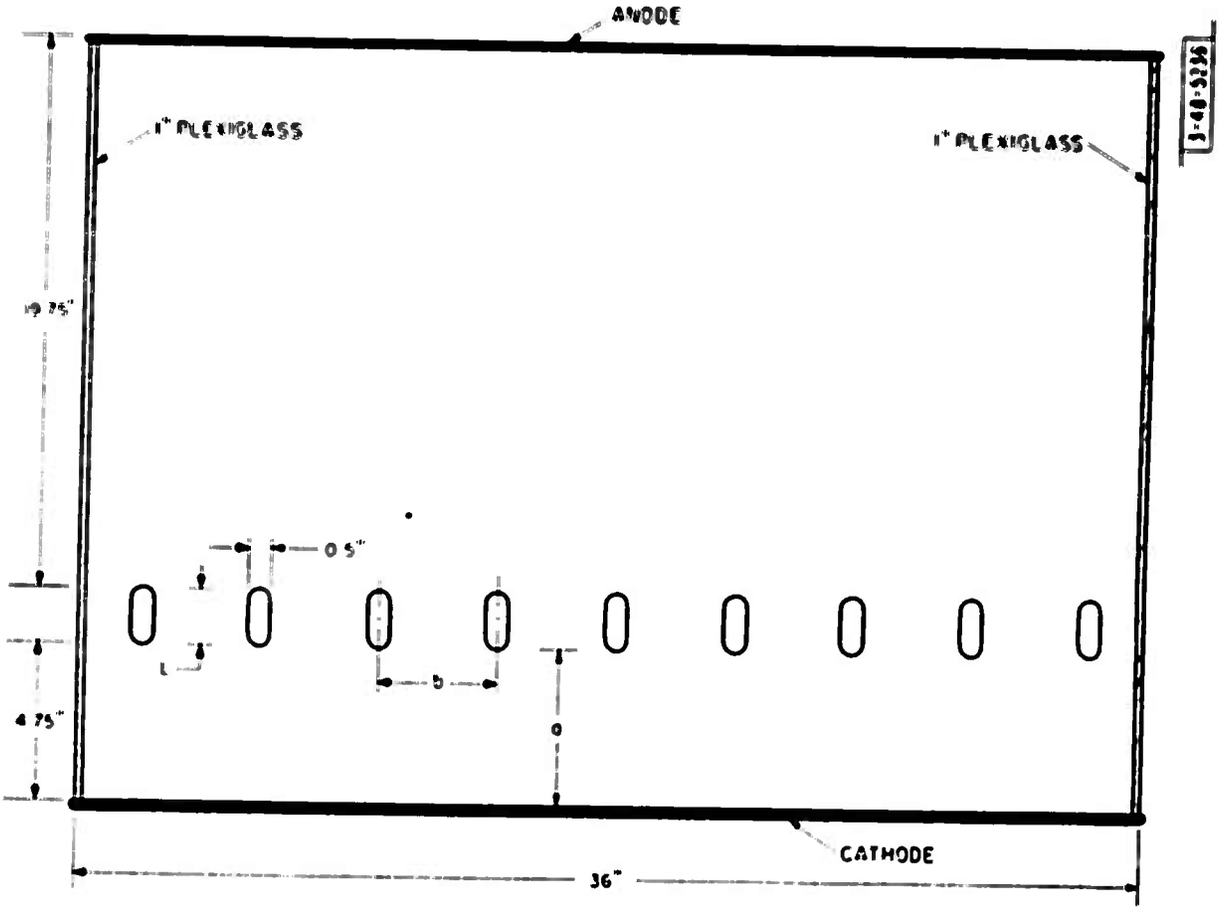

Fig. IV-3. Tank model of plane triode.

While waiting for the completion of the probes for trajectory plotting, it has been possible, using only the potential plotting circuits, to begin the investigation of a problem whose solution would have immediate application. Many proposed radar systems depend upon sophisticated pulse techniques which require the use of grid-controlled hard tubes. The power levels are such that it has been impossible to design conventional grid structures that are capable of dissipating the required power. An increase in the mass of the grid or a decrease in the grid interception current would be desirable, if neither change adversely affected the operation of the tube.

The only immediately apparent way of increasing the mass of the grid structure, without closing the grid spacing, is to increase the depth of the grid. This will enhance the effect of the grid, thereby increasing the amplification factor. It might then be possible to open the grid structure. Whether or not the decrease in grid interception due to opening the grid will be offset by added interception due to increased depth is one of the problems to be investigated. The first problem, however, is to find the effect of grid depth on gain, or cutoff voltage to which the gain is directly related.

A preliminary study of the effects of grid depth and spacing has started with a plane triode model in the electrolytic tank. The dimensions are given in Fig. IV-3. The first investigation was of the variation of cutoff voltage with varying grid depth and spacing. Five sets of grids varying in length (L) from 0.5 to nearly 7 inches were tested at grid spacings (b) varying from 4 to 16 inches. The results are shown in Fig. IV-4. It is easily seen that any given cutoff voltage may be maintained with wider spacing if the grid is elongated. It also follows that, for a given spacing, the cutoff may be decreased by elongating the grid. Examination of the curve b/a = 1.685 (where a is the grid cathode spacing) reveals that a tenfold increase in grid depth from 0.12a to 1.2a yields an increase of 20 to 1 in e_p/e_g from 7 to 140.

The cutoff voltage was assumed to be that grid voltage which resulted in an equipotential line, of the same potential as the cathode, situated within 1/8 inch of the cathode (Fig. IV-2) at the closest point. For the narrowest grid spacing considered (b/a = 0.843), grid depths greater than 0.4a were not

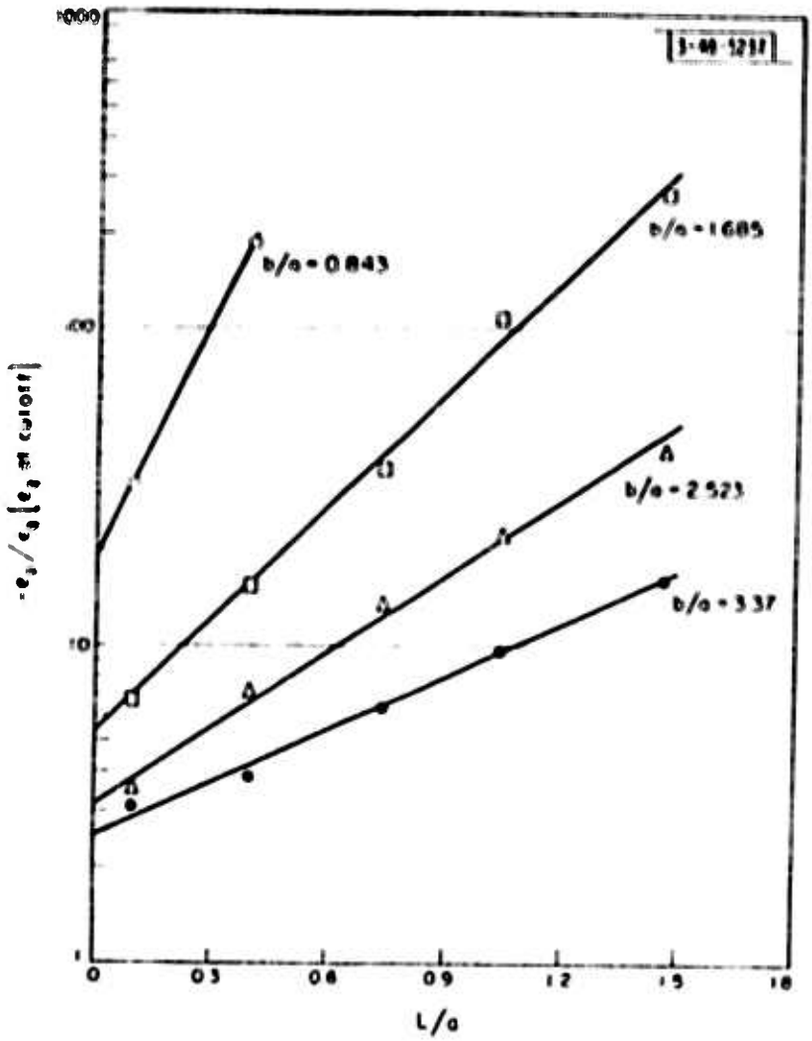

Fig. IV-4. Effect of grid depth on cutoff voltage.

considered, since the voltage gradient near the cathode was so small that an accurate determination of the cutoff voltage was impossible in the method used. For all measurements, the grid-to-cathode spacing was fixed. Since the cathode-to-plate spacing was fixed by the mechanical structure of the model, it was necessary to determine the potential at a constant distance from the grid and to use this potential as e_p in the calculation of e_p/e_g. This definition of e_p kept the grid plate separation constant for all cases and maintained the grid-plate perveance at a nearly constant value. The calculation of this potential was possible since, in each case, the gradient near the plate, out of range of the effect of the grid, was essentially constant.

W. A. Janvrin
M. E. Schwarz, Jr.

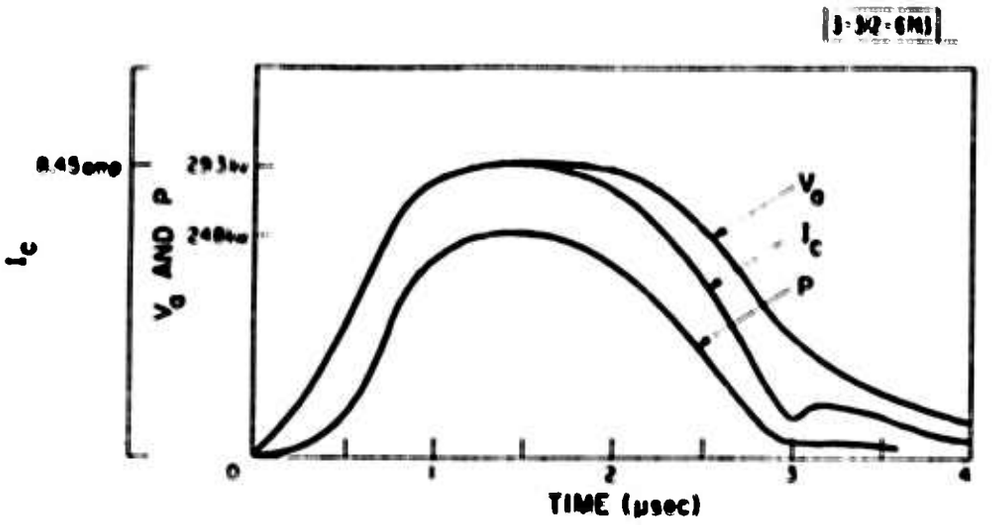

Fig. V-1. Pulse beam current, voltage and instantaneous power as a function of time.

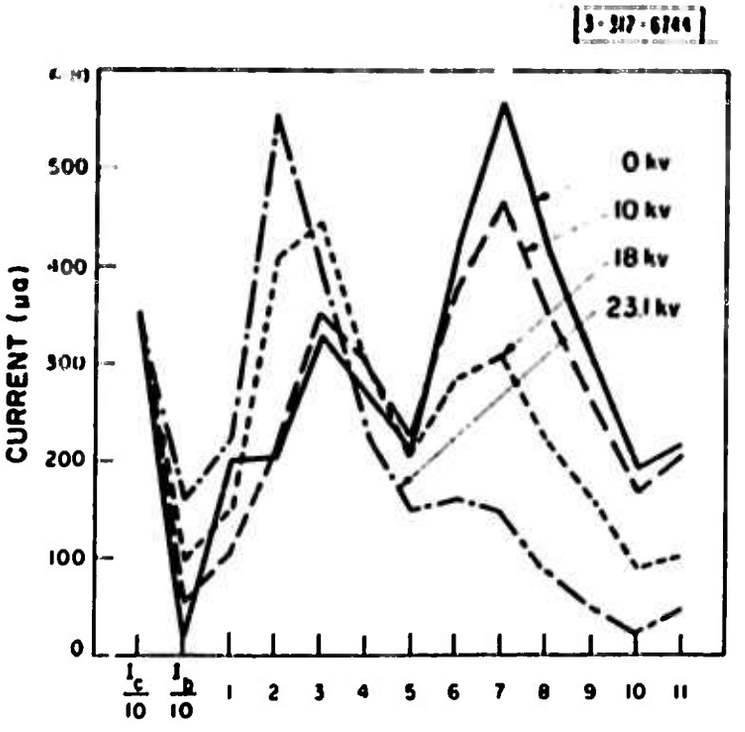

Fig. V-2. Plot of beam current to different collector rings as a function of bias voltage. The values of cathode and body currents are divided by ten.

V. BIASED COLLECTOR

The biased-collector project was established to investigate the characteristics of the spent beam of a klystron in the hope of obtaining information that would be useful in the design of multisegment biased collectors.

During the period covered by this report, a tube was completed and tests started. Before any significant amount of information was obtained, the cathode failed and the tube had to be reprocessed. The data reported below were taken on this reprocessed tube.

The experiments conducted to date have been with accelerating voltages below 35 kv, since it was desired to obtain some experience with the equipment at voltages low enough to permit operation in air. No data have as yet been obtained with RF drive on the tube. The measurements made have given an indication of the beam power delivered to the body, the collector and the collector-bias supply, for varying conditions of collector bias. The power delivered to the collector bias supply is of particular importance, since this represents power that might be recovered in actual biased-collector operation.

The experiments reported here were all conducted with a beam voltage of 29.3 kv. Figure V-1 shows the pulse beam current, voltage and instantaneous power as a function of time. The variation in perveance during the pulse is presumed to result from a drop in cathode activity during the pulse, since checks of the current and voltage-measuring circuitry revealed no inaccuracies therein.

The first measurements were made to determine the current distribution to the 11 collector segments, when all the segments were held at ground potential. The distribution in this case is indicated in Fig. V-2, which also indicates the variation in current distribution since all segments are biased negatively.

When all collector segments are biased to the same voltage, it is of interest to know the amount of power dissipated as heat in the body of the tube and in the collector rings, as well as the power delivered by the electron beam to the external DC power supply as a function of the common collector voltage. Because of the shape of the pulse, an appreciable amount of the beam power is carried by the electron beam at lower kinetic energy than that corresponding

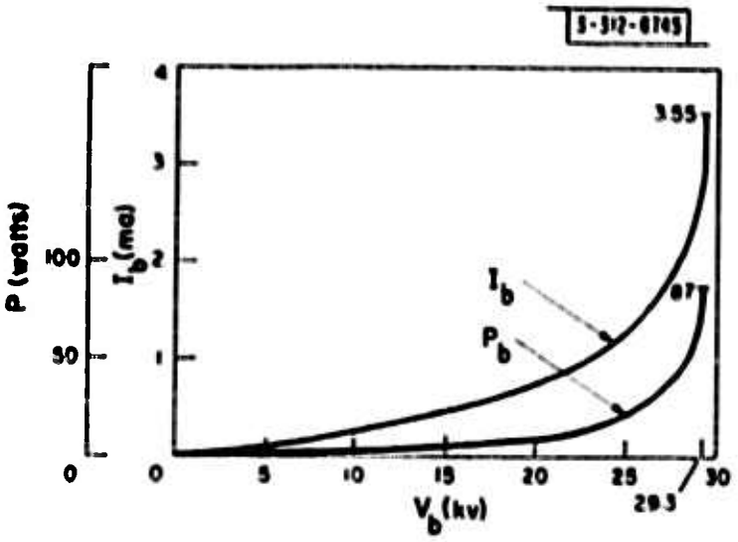

Fig. V-3. The body current and the corresponding power flow due to the imperfection of the voltage and current pulses as a function of the bias voltage.

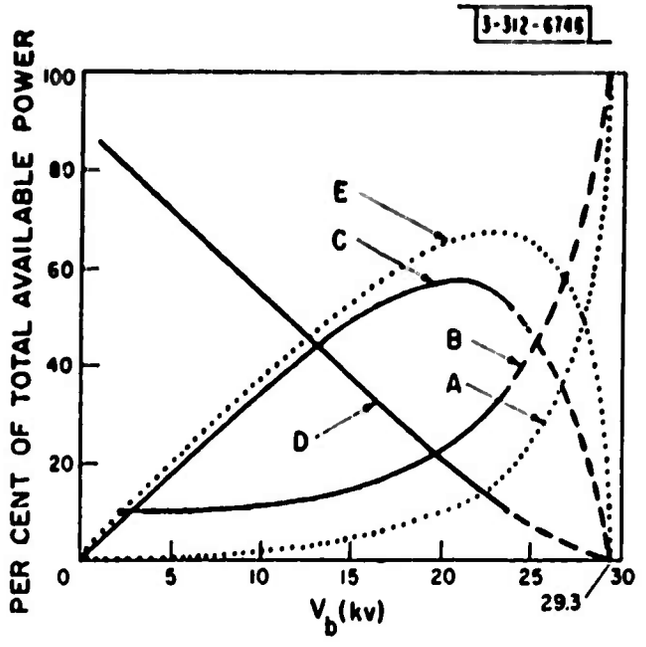

Fig. V-4. The distribution of power as a function bias voltage.

to maximum voltage during the pulse. This means that, for certain bias voltages, the part of the beam current which passes through smaller accelerating voltage than the collector-bias voltage must flow to the body of the tube. The measured body current on the meter must include this part of the beam current. The procedure for calculating the curves of Fig. V-3 was as follows. First, the power pulse of Fig. V-1 was obtained by multiplying the instantaneous values of the beam voltage and the current. Then the curves of Fig. V-3 were calculated by using numerical integration on the current and power pulses of Fig. V-1. These curves indicate the amount of current and the corresponding power carried to the body of the tube by that part of the beam which cannot overcome the DC bias on the collector rings because of the smaller accelerating voltage. Finally, the curves of Fig. V-3 were used to obtain the results given in Fig. V-4. For example, when all the collector rings were biased to −20 kv, the average cathode and body currents were 3.55 and 1.10 ma, respectively. From Fig. V-3 one finds that at least 0.72 ma of the cathode current must have gone to the body of the tube, since that much beam current is carried by the beam at an energy level less than 20 kv. The corresponding body power is 8.7 watts. (Curve A of Fig. V-4 is a replot of P_b of Fig. V-3.) The remaining fraction of the body current must then be of higher energy level than 20 kv. Since the energy distribution of this part of the body current (in our example, 0.38 ma) was not known exactly, it was assumed to be of the highest energy possible, that is, 29.3 kv. Therefore, the curve of the dissipated power in the body of the tube, as shown in Fig. V-4, curve B, gives an upper bound for this variable. Curve C, representing the power delivered to the DC power supply is the difference between the average cathode and body currents times the common bias voltage on all the collector rings. The difference between the total beam power and the sum of power delivered to the external bias supply and the body power is assumed to be dissipated as heat in the collector. This thermal energy is plotted as curve D in the figure. Curve E represents power that would be delivered to the bias supply if the body power were the minimum theoretical value indicated by curve A (that is, no primary body interception).

The dotted curves in Fig. V-4 show the best possible operation of the collector, and represent the lower bound for the power dissipated in the body of

the tube and the upper bound for the power delivered to the power supply, which is possible with pulses of the shape shown in Fig. V-1. The dashed part of the experimental curves of Fig. V-4 represents an extrapolation of data obtained, since it was not considered prudent to increase collector bias to the point where all the beam current was returned to a small portion (possibly) of the tube body.

Following the measurement with all rings at the same voltage, the rings were separated and the voltages adjusted so that the bias varied monotonically from −10 kv on the first ring to −19 kv on the last ring. With these voltages, the power delivered to the bias supply was essentially the same (57 per cent) as it was when all the rings were at −20 kv. However, when all rings were at −20 kv, the current delivered to the tube body was 85 per cent higher than it was with the graded voltage arrangement.

The above example does not necessarily represent the best possible operation of the segmented collector. The objective of future work along these lines will be to optimize the biasing schedule so as to maximize the power delivered to the external circuit and minimize the body power.

During the next six months it is expected that the low-voltage tests of the multisegment collector, including the RF tests, will be concluded and work will begin on either intermediate or rated pulse voltages. These tests will have to be conducted under oil.

A. Saharian

VI. CATHODES

Tests have been made on a group of six planar diodes purchased from Sperry Gyroscope Company.[2] These diodes are designed for studies of cathode materials. The cathodes of the six diodes tested thus far were converted by Sperry, and activated at 900°C for three hours at an anode voltage of 4 volts. Another six diodes are completed up to the cathode conversion, which we plan to do ourselves (see below). Attached to each diode is a 1-liter/sec ion pump, which serves principally as a vacuum gauge.

The purpose of these tests is to get an idea of what sort of emission can be obtained from oxide-coated cathodes under good vacuum conditions. At present there is a large gap between industrial design values of emission (about 1 amp/cm^2) and values reported from laboratories (up to 130 amp/cm^2).[3] A hoped-for result of this work is to bring the design value closer to laboratory values. Since the question of composition of the coating is not of interest at this time, we are using a standard triple-carbonate mix, RCA 33-C-118. In order to avoid variable effects of different activators in the cathode base, we are using passive bases. In each group of six diodes, three have bases of 499 nickel, three of platinum.

The diodes are pulsed by a pulser capable of generating pulses up to 14 kv peak. The pulser is provided with a device for automatically scanning up and down in voltage. One complete scanning cycle takes 20 seconds. The voltage and current pulses are fed into the horizontal and vertical inputs, respectively, of an oscilloscope, resulting in a display of the I-V curve on the screen. The reticule in front of the screen has a three-halves-power-law curve inscribed on it.

In the initial tests, the nickel-based cathodes seemed to be the more active, but the statistical sample is small enough that we hesitate to make a definite statement about the relative merits of nickel vs platinum as a base material at this time. However, the tubes fell into two groups with respect to activity, with distinctive properties:

(a) Two, nickel-based, of high activity (maximum space-charge-limited current density, about 15 amp/cm^2 peak).

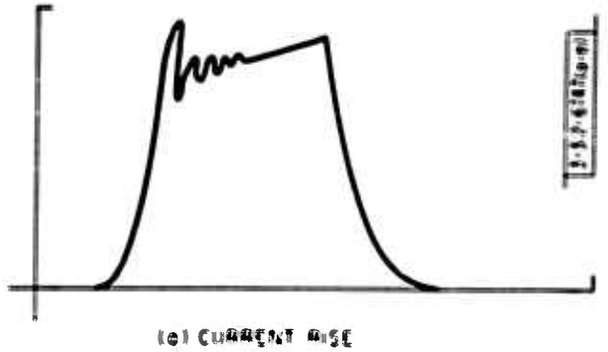

(a) CURRENT RISE

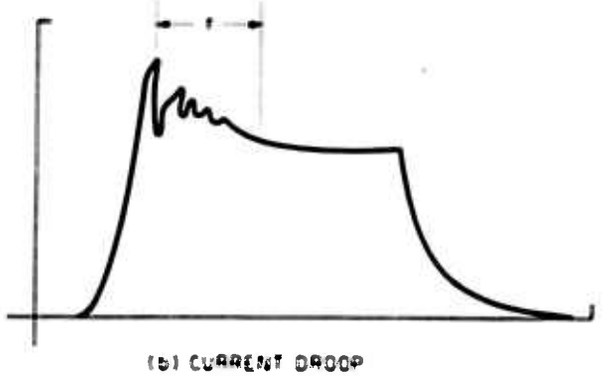

(b) CURRENT DROOP

Fig. VI-1. Current pulses.

(1) The most active one showed a current rise [Fig. VI-1(a)] during the pulse over the entire range of voltages used in the test.

(2) The next one showed a current rise at medium voltages (i.e., within the space-charge-limited (s-c-l) region), but a current droop [Fig. VI-1(b)] in the saturation region.

(b) Four of low activity (maximum s-c-l current density, about 4 amp/cm^2 peak).

These four all showed a pronounced current droop in the saturation region. One tube showed an effect in the first tests which was not repeatable later, namely, a long-term current decay. The evidence was that, in the saturation region, the current for a given voltage was lower by about 3 per cent on the down-trace of voltage than on the up-trace [Fig. VI-2(c)].

This same tube was tested for variations of maximum s-c-l current with pulse width and repetition rate. No effect was found by varying pulse width from 1 to 10 μsec at two different repetition rates. A variation of the repetition rate from 50 to 6000 cps caused a decrease of 25 per cent in the current (Fig. VI-3). This behavior is to be expected in a tube that shows a long-term decay but no short-term droop.

Figure VI-2 shows the I-V curves for the various conditions. For the short-term rise and droop effects, the curves look similar, showing a fanning-out tendency in the saturation region, except that the patterns at the end of the fan differ. Each pattern is merely a representation of the current pulse turned on its side, and it shows the ringing at the beginning of the pulse. By noting the position of the ringing pattern, one can tell whether the lower current (lower trace) came before or after the higher current in time. A representative photograph is shown in Fig. VI-4.

The short-term current decay is exponential and has a time constant of about 3 μsec. Figure VI-1(b) represents a 10-μsec pulse. The decay presumably results from the depletion of a hyperactive surface layer, after which the emission settles down to a rate determined by the activity of the bulk of the coating.

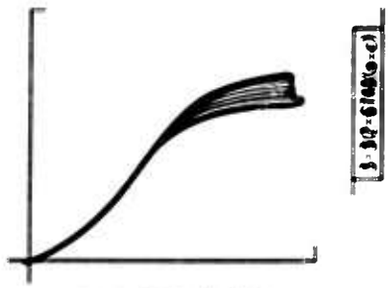

(a) CURRENT RISE

(b) CURRENT DROOP

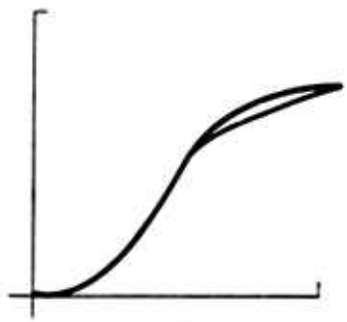

(c) LONG-TERM DECAY

Fig. VI-2. I-V curves.

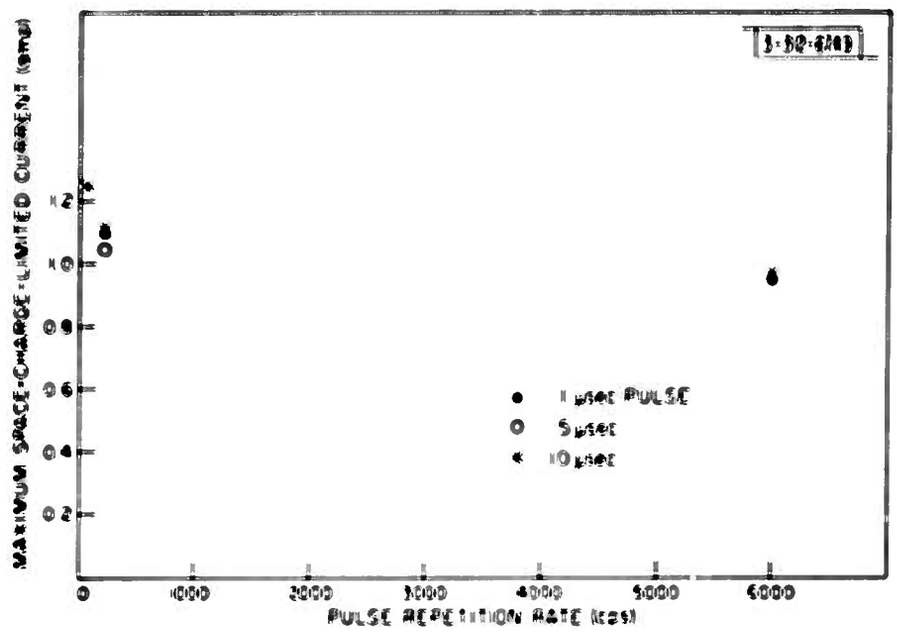

Fig. VI-3. Maximum s-c-l current decrease with increasing repetition rate.

Fig. VI-4. I-V characteristic showing current decay during pulse.

The short-term current rise was assumed to be an indication of a temperature rise during the pulse. (The temperature rise corresponding to the observed 10 per cent rise in current would be about 5°C.) On this assumption, observations were made with a photoelectric pyrometer, and they are described below. The conclusion was that the temperature rise, if any, was less than what the pyrometer could detect, i.e., less than 5°C. Later calculations all point to a likely temperature rise during a pulse of less than 0.1°C, and most recent tests indicate that the current rise may not be a temperature effect at all.

We have looked for temperature rise in the cathode during the pulse, using a photoelectric pyrometer similar to the one described by Silverman.[4] The first measurements indicated large temperature rises, of the order of several hundred degrees. Calculations convinced us that this was impossible. To locate the trouble, we took measurements with a series of infrared filters that have different short-wavelength cutoffs interposed between the tube and the pyrometer. We also compared the responses of two phototubes, one peaked in the visible and one in the infrared. The results showed that the radiation that we were looking at was peaked in the visible. A visual inspection showed that indeed there was a bluish discharge, which seemed to originate from the anode. The discharge was not uniform, but stringy. The strings were stationary, not only during one period of pulsing, but also after repeated turning of the pulser on and off. Bright bluish spots appeared on the anode at the starting points of the brighter strings. As the voltage was reduced, some spots persisted even after the general discharge could not be seen.

Tests to date have been limited, and it is possible that the observed effect is a transitory one. However, certain interesting possibilities suggest themselves.

(a) The strings may result from the patchy emission from the cathode. This would explain the stationary feature.

(b) With the pressures around 10^{-8} mm Hg existing in the tubes, it is hard to see how this discharge could exist in the residual gas. The bright spots may indicate regions of intense local heating. It is interesting to speculate whether or not copper is being vaporized from the anode at these points, and is producing the discharge. We plan to look at the spectrum of the discharge to find more about the mechanism.

We have vacuum-converted the cathodes in a series of nine small diodes, and now have the procedure stabilized to the point where the tubes behave consistently. We next plan to convert a series of cathodes in hydrogen, following the suggestion of MacNair,[5] to establish our procedure in this technique. The technique will then be adapted to hydrogen processing of the second set of six Sperry diodes, whose properties we can then compare with those that have been vacuum processed.

H. A. Pike
F. T. Worrell

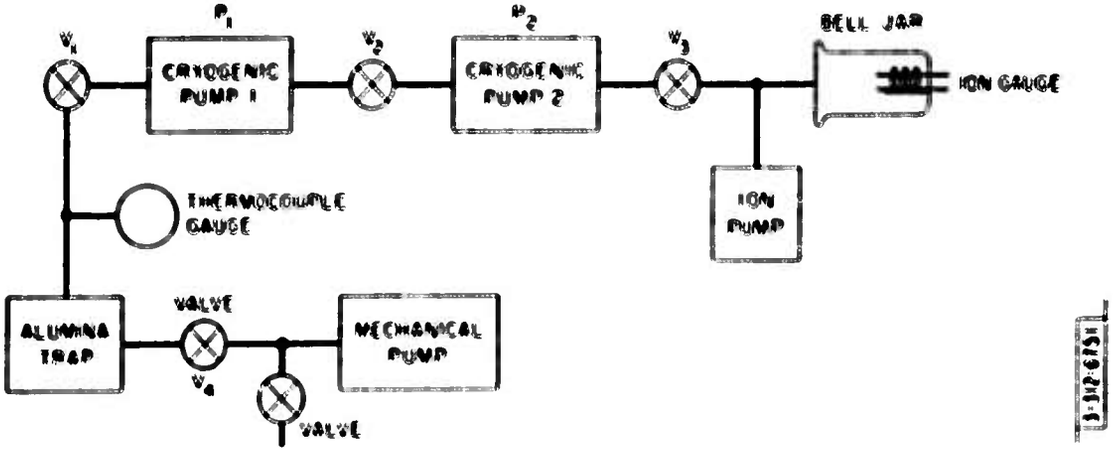

Fig. VII-1. Cryogenic pumping system.

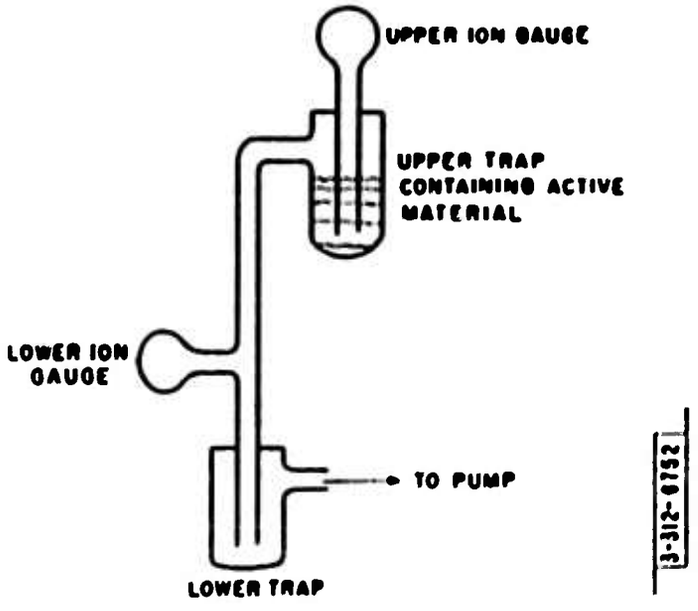

Fig. VII-2. System for testing alumina and zeolite.

VII. VACUUM TECHNIQUES

A. CRYOGENIC PUMPING SYSTEM

Initial tests have been run on the cryogenic pumping system mentioned previously.[6] The design follows one suggested by Feinleib,[7] and is shown in block diagram in Fig. VII-1. The mechanical pump reduces the pressure to the low micron range initially, thus reducing the pumping burden on the cryogenic pumps, and allowing them to pump to lower pressures than if they started from atmospheric pressure. The advantage of cleanliness, characteristic of the cryogenic system, is preserved by inserting the alumina trap between the mechanical pump and the rest of the system.

The system is first pumped down to about 10μ with the forepump, valves V_1 through V_3 are open, and V_3 is then closed. The alumina is conditioned by heating the trap and pumps P_1 and P_2 to 500° to 600°C while the forepump is running. When the pressure has dropped to about 100 to 200μ after outgassing, the heaters are turned off. It is generally found that, when the alumina is at room temperature and V_4 is closed, the pressure at the trap is lower than that at the pump. The remaining steps consist of closing V_1, chilling P_1 till it has pumped down, closing V_2 and chilling P_2. When the pressure has attained its lowest value, the ion pump is turned on. When closing V_3 causes the pressure to drop, V_3 is left closed, and the ion pump takes over. In preliminary experiments, we have been able to attain pressures as low as 1.5×10^{-7} mm Hg with the cryogenic pumps, before turning on the ion pump.

The present pump design is too massive. It takes too long to heat the alumina, and the pumpdown is so slow as to suggest that it is restricted not by the conductance of the pumping line, but rather by the rate at which the alumina can be cooled. An improved pump is under construction.

Comparative tests have been made on the conditioning of small amounts of activated alumina and zeolite in a system pumped by a 25-liter/sec oil diffusion pump (Fig. VII-2). The activated alumina (Alcoa type H151) was preconditioned by baking in air at 450°C for two hours, and then put into the vacuum system. The system was then pumped down. When the temperature had been raised slowly over a period of six days to 250°C but with no success at getting the pressure below 1μ, we stopped the series of tests.

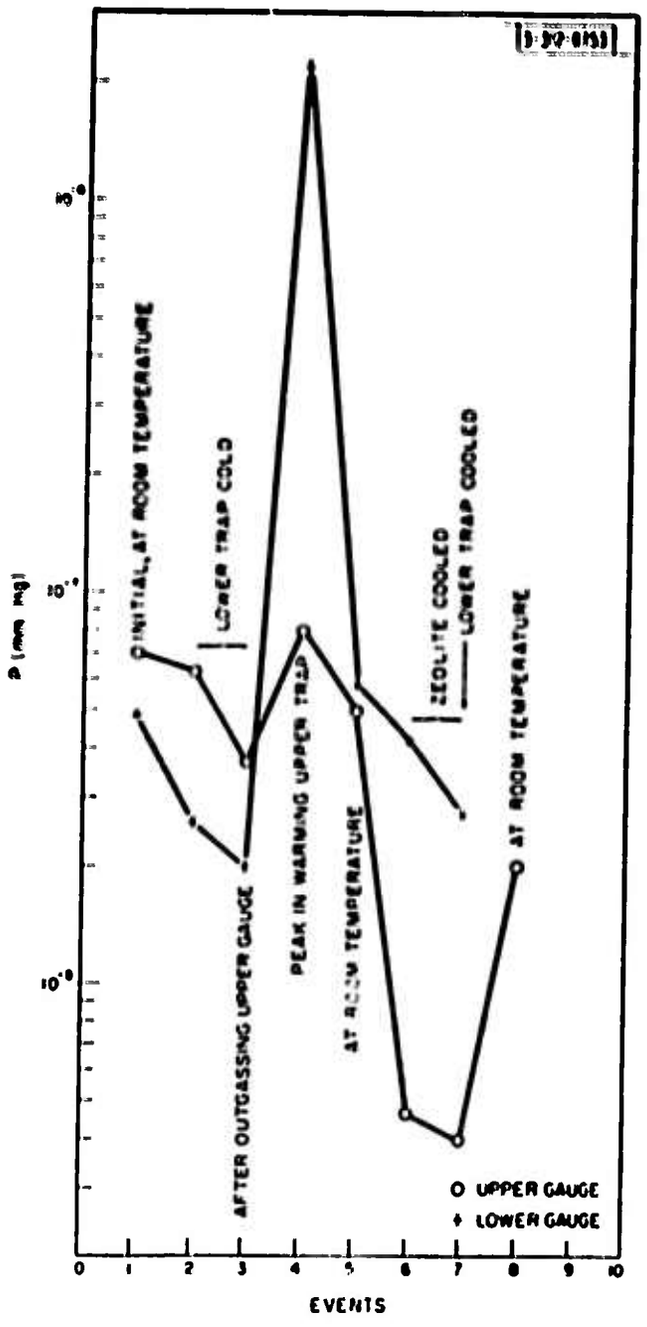

Fig. VII-3. Summary of tests on zeolite.

Zeolite, Type 13-X, was substituted for the alumina. Preconditioning in this case consisted of baking for 7 hours at 450°C with dry nitrogen flowing through. The system was cooled, and the pumps turned on. The temperature was run up to 450°C in 24 hours without exceeding 1μ and, after 30 hours at 450°C, the pressure was 2×10^{-4} mm Hg.

After a period of ten days at room temperature, during which period the gauges were outgassed, the upper gauge read 7×10^{-8} mm Hg, the lower gauge 4.9×10^{-8}. (Since the two gauges are not comparable, no attention should be paid to their relative readings, only to changes in readings.) When the lower trap was refrigerated to liquid nitrogen temperature, the lower gauge reading dropped by a factor of 2.0 and the upper gauge by a factor of 1.1 (Fig. VII-3). The zeolite trap seems to be effective in isolating the system from the pump, in accord with the report of Harris.[8] When the lower trap was warmed, the pressure went up, showing several bursts of vapors, with the upper gauge being much less affected than the lower. The final steady reading of the upper gauge was 25 per cent lower than it had been before the cooling of the lower trap, suggesting a permanent removal of gases from the zeolite during the cooling period.

When the zeolite-filled trap was cooled, the lower gauge reading went down by a factor of 1.4, the upper gauge by 10, as a result of the pumping action of the zeolite. Cooling the lower trap brought the upper gauge reading down slightly, as earlier. Some 12 hours after warming the system to room temperature again, the upper gauge read appreciably lower than before, probably because gases had been trapped permanently in the zeolite. The results are summarized in Fig. VII-3. Note that the time scale is not linear, but records events.

Further tests are being made on zeolite in smaller amounts suitable for traps in small systems. Comparable gauges will be used, to give us more information.

B. ION GAUGE POWER SUPPLY

Commercial power supplies for ionization gauges give insufficient information to the investigator of these gauges, and provide insufficient flexibility

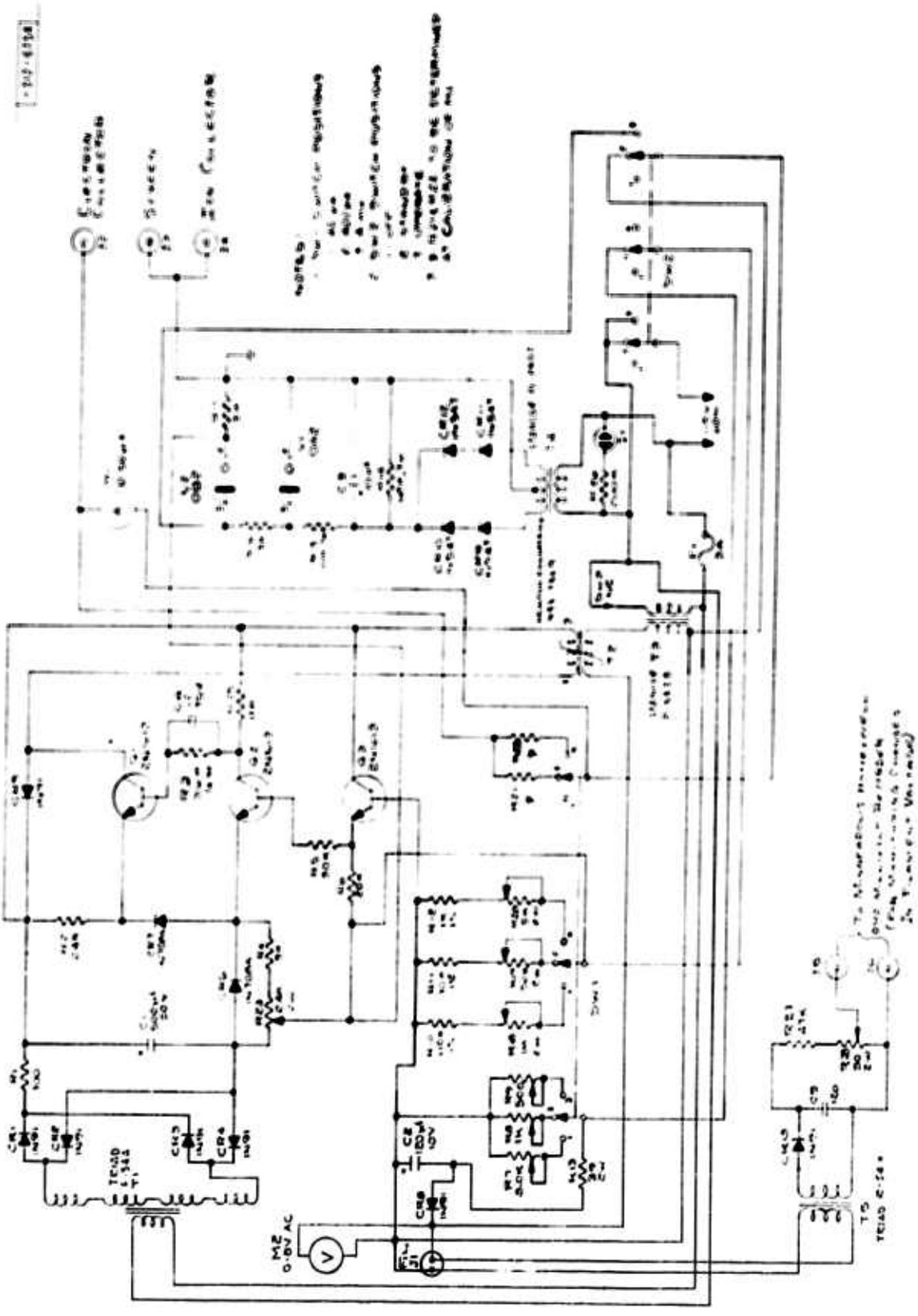

Fig. VII-4. Schematic diagram of Nottingham gauge power supply.

of operation. We have designed a power supply with the following properties of interest to us.

(1) The electron current can be stabilized to any one of three values, nominally 4 ma, 400 μa and 40 μa, available in a selector switch.

(2) A "standby" circuit which allows the filament to run at operating temperature while the accelerating voltage is off.

(3) Provision for turning off the filament while the electrode voltages stay on.

(4) A meter to monitor filament voltage

The standby setting allows one to turn the gauge on and off without introducing the gas burst from the filament at turn-on. The third provision allows a check of the ion collector current, to see how much, if any, is leakage from other electrodes. The filament meter is included, because it has been found that the filament itself is a fairly sensitive indicator of changes in vacuum conditions, under favorable vacuum conditions the emission from the filament improves, whereas a worsening of the vacuum can, under some conditions, produce a large drop in emission efficiency. Where the electron emission is stabilized, these effects show up as a drop or a rise, respectively, in the filament voltage and current. The voltage changes more than the current.

The power supply (Fig. VII-4) consists of a filtered DC source with two shunt regulators arranged to provide +135 volts to the electron collector and +30 volts to one side of the filament. This permits the screen to be grounded and the ion collector to return to ground through the high impedance of a Keithley electrometer.

The electron collector current is monitored, and the monitor automatically adjusts the filament power to maintain the electron collector current constant to any value determined by the operator. The automatic control operates as follows. The electron collector current flows through R_{10}, R_{11} or R_{12}, depending on the current range chosen. The resultant voltage drop is the base voltage of the emitter follower Q_3. The emitter voltage of Q_3 is compared with a Zener reference voltage. A voltage in excess of the Zener voltage produces a base current flow in Q_2 which is amplified in Q_2 and Q_1. The circuit

is arranged so that an increasing current in Q_2 causes a decreasing current to flow in Q_1. The current flowing in Q_1 flows through the control winding of a saturable reactor whose gate windings are in series with the filament supply of the vacuum gauge. The gate winding reactance is maximum when the control current is zero. The control loop is thus closed by the saturable reactor.

When in the stand-by mode, a DC voltage proportional to the filament AC voltage is compared with the Zener reference voltage, and regulation of the filament voltage in the absence of electron collector current is achieved through the same chain of events described above. Several of these units are now being tested with various gauges.

F. T. Worrell
W. A. Janvrin

VIII. VOLTAGE BREAKDOWN

Vacuum voltage breakdown measurements were resumed in the last quarter and are now proceeding on a full-time basis.

The initial work on gap breakdown previously reported showed that experimental copper electrodes could be conditioned by low-energy breakdowns, causing their voltage holdoff capability to double. This conditioning will be investigated with an electrode assembly which has four anodes and four cathodes. Careful electrode conditioning, followed by changing one electrode without breaking the vacuum, will allow observations to be made on the effects of both anode and cathode conditioning. Another feature of this assembly will allow the preparation of the electrode surfaces by vacuum-depositing fresh layers of copper and then positioning them for breakdown measurements.

Vacuum voltage breakdown across high-voltage insulators is also being investigated. Experience with some high-power microwave tubes has shown that, when an insulator is in the vicinity of a high-power electron beam, its voltage holdoff can be both poor and unpredictable.

An experiment to determine if one can raise this holdoff voltage has begun, using steatite cylindrical pillar insulators. They are one inch long by $\frac{1}{4}$-inch diameter and at 10^{-5} mm Hg holdoff from 35 to 45 kv DC. When the insulator is coated with chromic oxide in a silicate binder and then baked, holdoff is increased to 55 to 70 kv. The end points of the breakdowns coincide with very narrow gaps between the insulator base and the stainless steel support plates. The large voltage gradient across this gap initiates a spark which then triggers a breakdown along the insulator.

To eliminate this triggering, a second insulator, in addition to chromic oxide, had an aquadag coating on each end, thus eliminating any voltage gradient across the gap. This insulator held off more than 110 kv DC. For comparison, an insulator with just the aquadag on each end and no chromic oxide broke down at 30 kv (the thin edge of the aquadag coating results in a very large voltage gradient).

The significant increase in holdoff voltage due to the Cr_2O_3 coating can probably be ascribed to the decreased surface resistivity of the coated insulator. The uncoated insulator resistance of 10^{15} ohms fell to 10^{13} ohms after coating. The decrease in surface resistivity helps to establish a more uniform voltage gradient along the surface and allows a higher voltage to be applied across the insulator before a gradient large enough to cause a spark is reached.

Additional tests are being made on insulators whose surface resistivity has been further lowered to 10^{11} ohms by the addition of aquadag to the chromic oxide. The tests described were made on steatite since it was readily available. Further measurements of coating techniques on alumina will also be made.

A. Vierstra

IX. MEASUREMENTS OF SURFACE CURRENTS IN KLYSTRON CAVITIES BY THE PERTURBATION OF RADIATION FIELD

A new, indirect method for measuring the absolute field strengths on the boundaries of a microwave resonator has been developed. This method is based on perturbation of the radiation field, and is useful in applications where the other indirect methods, which are based on perturbation of the mode field, fail or become laborious and inaccurate.

The new method was used to determine the distribution of the ohmic losses on the four walls of a klystron reentrant resonator. The results were reported in the last Semiannual Technical Summary Report and are shown in Fig. IX-1.

The method was also used to measure the distribution of the surface current on the drift-tube wall of the resonator (wall 1). At the time of these experiments, some work was done on the stalo (see block diagram of Fig. IX-4 in the last Semiannual Technical Summary Report) to improve the frequency stability of the system, which resulted in changing the stalo frequency range. It was then necessary to change the resonator dimensions in order to have the resonant frequency fall in the stalo frequency range. This change was accomplished by increasing the length of the drift-tube wall from 0.300 to 0.324 inch. This increase in wall length resulted in the increase of its losses from 15.3 to 19.4 per cent. Thus the main purpose of the new experiments was to determine how the 19.4 per cent of the total energy dissipated on the resonator walls is distributed on the drift-tube wall.

In these experiments the spraying technique was used to change the wall surface impedance. The idea was to spray the total wall surface area to a thickness of about 0.002 inch (several times the skin depth). The coating was then machined off all the surface except for an annular ring where the field strength was to be determined. When a large number of measurements was required, such as in the case of plotting the field distribution over all the surface, this method was found to be rather laborious, and another method was used. In the second method, the surface impedance at the place where the field had to be determined was changed from that of sprayed material to that

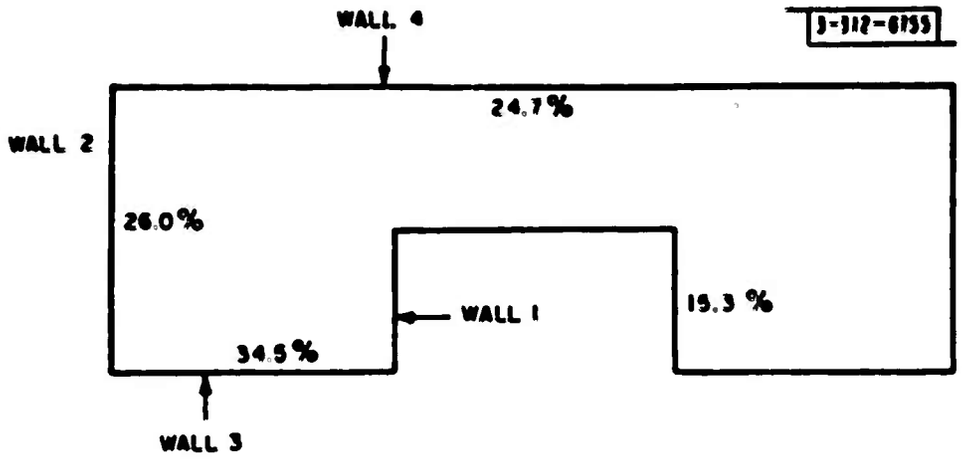

Fig. IX-1. Average ohmic losses on the four walls of cylindrical reentrant resonator.

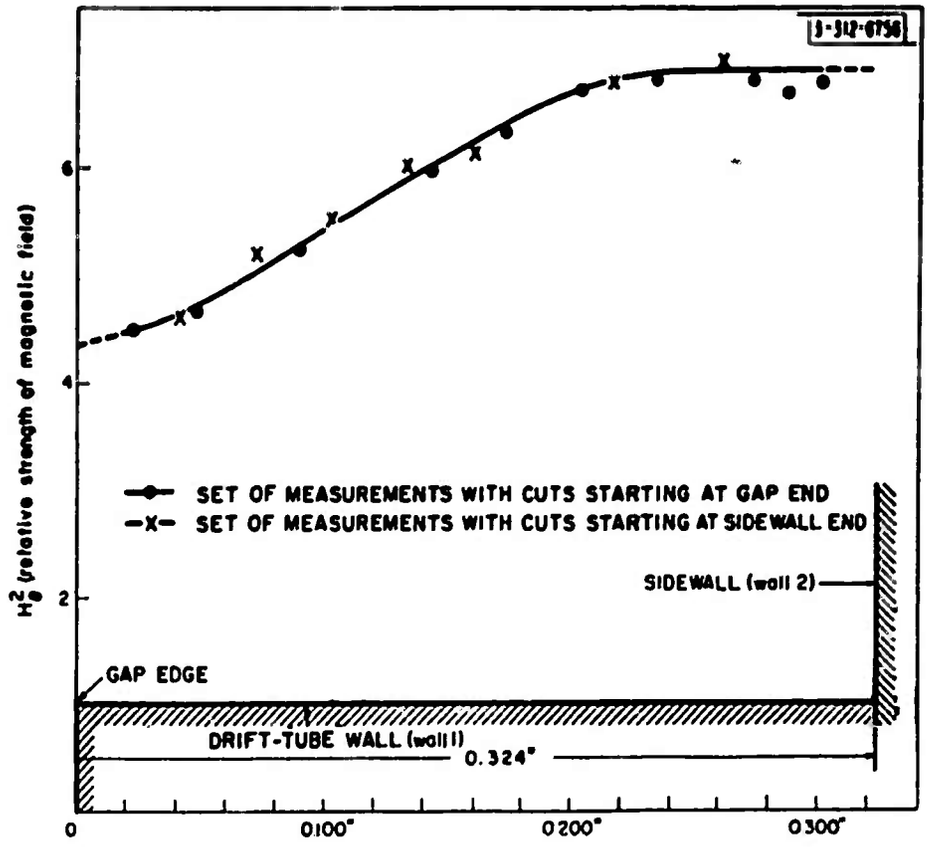

Fig. IX-2. Surface field distribution on the drift-tube wall of reentrant resonator.

of copper (the base metal) which is the inverse of the first method. The procedure for plotting the field distribution was as follows: Starting with a surface completely sprayed, a narrow annular ring of the coating (about 0.030 inch wide) was machined off one side. The resonator Q's were measured before and after machining off the ring, and the difference between the two values gave a measure of the local field strength at the ring. The width of the machined ring was successively increased and the Q measured each time, until all the coating was machined off. To check the results, two sets of measurements were taken on two identical walls sprayed with TiC. In the first set of measurements, the cuts were started at the gap edge of the wall and in the second set the cuts were started on the other end. The results of these experiments are shown in Fig. IX-2.

With these experiments, the work on this project is concluded.

I. Hefni
M. Nader

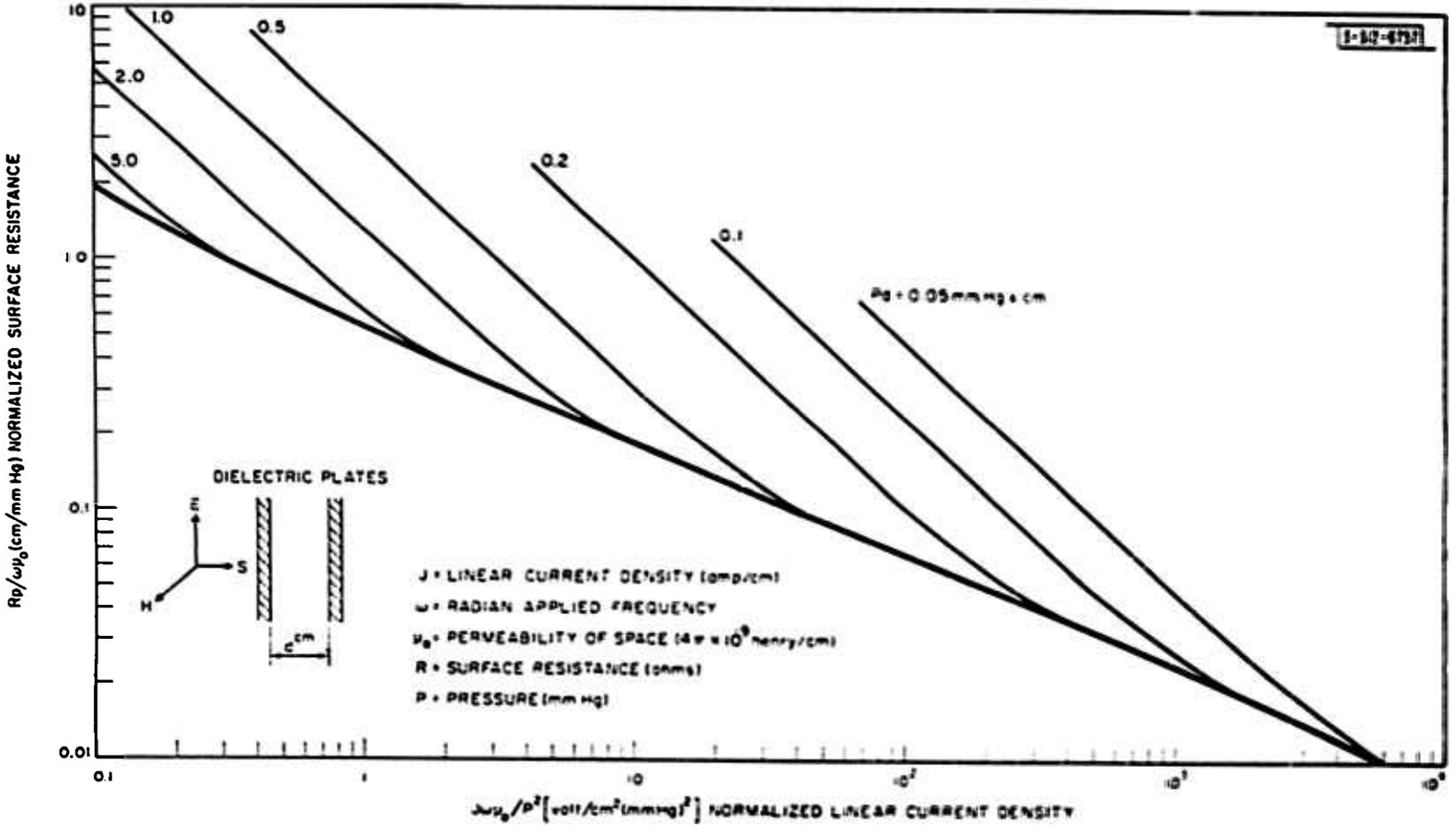

Fig. X-1. Computed surface resistances of argon discharge between dielectric plates.

X. DUPLEXER INVESTIGATIONS

A. CALCULATION OF ARC LOSS IN FOLDED CYLINDERS

It has been reported[9] that, for microwave discharges, the component of electric field in phase with the current is equal to the sustaining field in a DC discharge at low current levels. At higher current levels the conductivity of the plasma is sufficient to shield the RF fields from the interior of the discharge. This is an example of the "skin effect." Calculation at high current levels is very complicated because the electric field, the electron density and the electron temperature all vary with depth into the discharge. The electron production and loss equation, together with Maxwell's equations in a conducting medium, had to be solved simultaneously. These equations contained coefficients involving ionization and rates of diffusion which varied with the electric field. These coefficient functions were evaluated from theoretical and experimental DC data. The problem was put into an IBM 7090 computer together with the proper boundary conditions and the results are shown in Fig. X-1.

The ordinate in this graph is the normalized surface resistance and the abscissa is the normalized linear current density. The series of lines of slope minus one for different pd values represent lines of constant ordinate, times abscissa or constant E/P, and represent the low current case. At higher currents these lines all merge into the heavy double line which represents the highly shielded case.

B. APPLICATION TO L-BAND FOLDED CYLINDER

The design of an L-band duplexer cavity was mentioned in the last Semiannual Technical Summary Report. A quartz folded-cylinder TR tube of 1.100-inch diameter is mounted horizontally in a capacitive iris across a rectangular cavity. The results of the machine computation have been applied to this L-band duplexer with the results shown in Fig. X-2, which is a plot of the average power-handling ability of the cavity as a function of duty cycle when the hottest point in the tube is at 450°C. The lines approaching a slope of minus one represent the unshielded case. The line of slope approximately minus 1/3

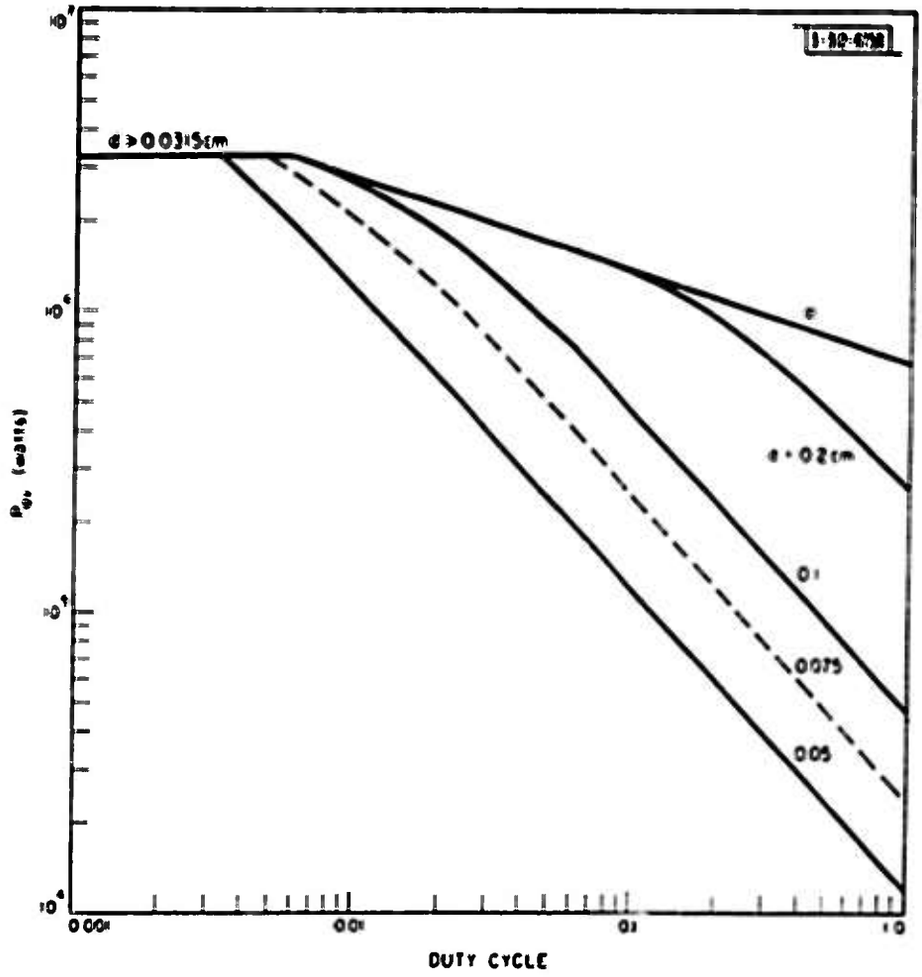

Fig. X-2. Computed average power-handling ability of L-band cavity.

(marked ∞) represents the shielded case. The machine computation mentioned above does not take into account the electron-positive ion collisions which tend to produce a constant value of conductivity (equal to that in a fully ionized gas) in the discharge at high current levels. This case is represented by the horizontal line and holds for cases where the tube gap is greater than the skin depth (0.0315 cm) in a fully ionized gas.

The gap actually used is 0.075 cm; hence, for duty cycles larger than 0.01, the discharge is unshielded and the electric field is constant. In this case the power dissipated in the tube should be proportional to $\sqrt{P_{av} D_u}$ so that the temperature rise at the hottest point in the tube was plotted against this quantity as in Fig. X-3. The crosses are for data taken at high peak power, low duty cycle in the resonant ring (maximum 10 Mw peak, 0.003 duty) and the circles are for data taken with a CW magnetron. The lower portion of the curve has a slope of plus one, whereas the upper portion shows a lower temperature rise for a given amount of heat input. At high temperatures a large fraction of the heat is lost by radiation which follows a T^4 law. At 450°C and a duty cycle of one, the measured average power is 31,300 watts, whereas the calculated value is 24,000 watts. The figure also shows that, at the higher duty cycles, the gap spacing could be increased to give an increase in power-handling ability at the expense of an increase in recovery time (100 μsec with 0.075 cm gap and 1 mm Hg argon). No cooling is used at present.

It was decided to design a balanced TR duplexer since it requires only one high-power switching tube. The dimensions for a dual TR mount have been determined and a final duplexer with tuners and pressurization is being designed. Electrical measurements are being taken to determine the proper shape for a post-TR cavity using a metal-ceramic TR tube to protect the receiver from leakage past the pre-TR.

C. S-BAND TR WINDOWS

The Brush Beryllium Company (Cleveland, Ohio) has accepted an order to manufacture several S-band TR windows which use beryllium oxide. These TR windows may be described as flattened-out folded cylinders, since the discharge takes place in a narrow (0.015 inch) void in the dielectric so that diffusion is

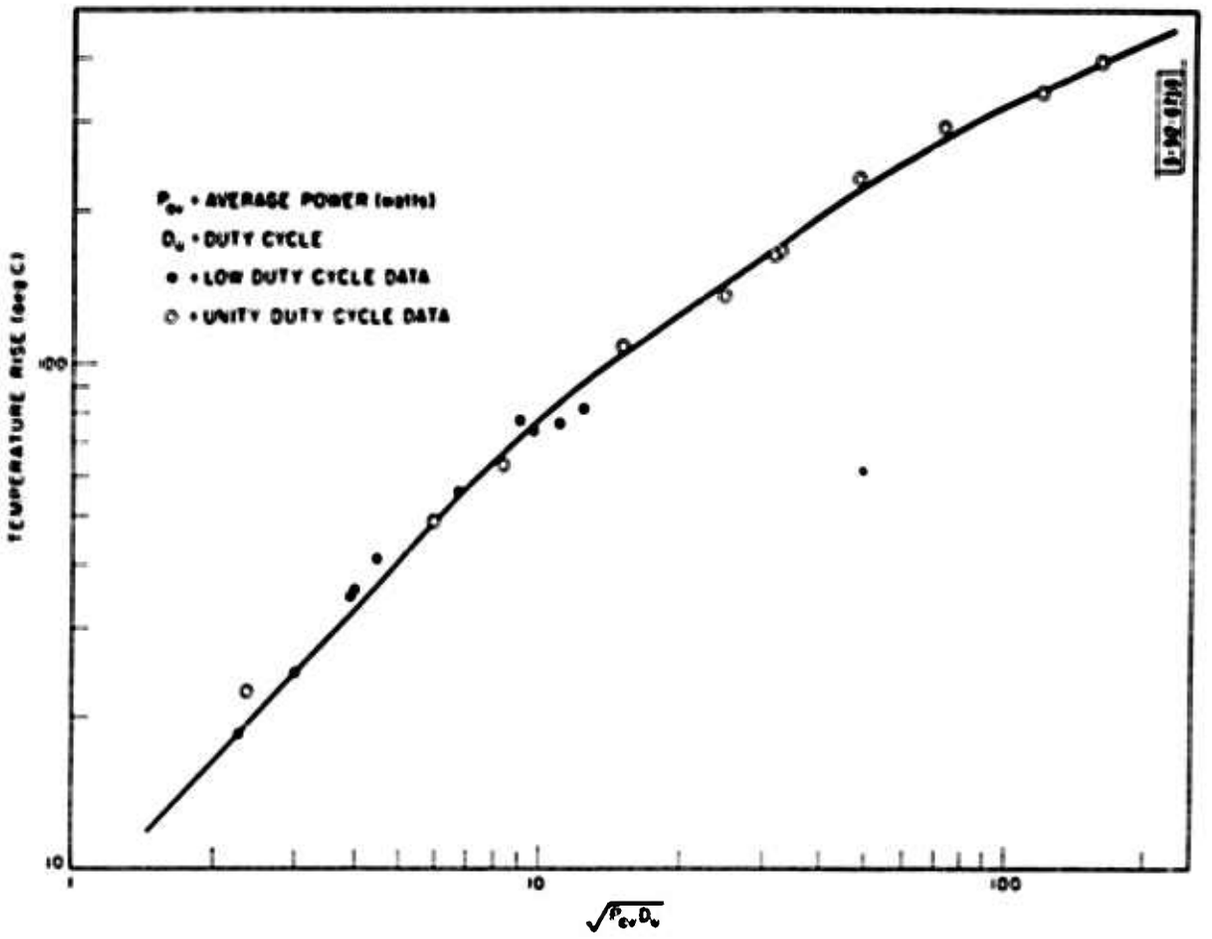

Fig. X-3. Temperoture rise for L-band folded-cylinder TR tube.

used as a recovery mechanism. Much attention has been directed to designing for best heat flow, so the TR tube should handle several hundred kilowatts of average power. These windows will be incorporated in an RF structure which is being designed at Lincoln Laboratory.

D. S-BAND HIGH-POWER TEST EQUIPMENT

A high-power S-band traveling-wave resonator has been built and tested at Dielectric Products Engineering Company. This unit, which will be delivered early in January 1962, gives a CW gain of 13.5 to 14.5 db and should enable simulation of an average power of about 0.5 Mw, using the Litton pulsed klystron (5 Mw peak, 50 kw average) which is scheduled for delivery in late January 1962. Modifications to the existing modulator are also planned to provide pulse widths up to 30 μsec. It is expected that high-power S-band tests can begin about 1 April 1962, provided there are no further delays in equipment delivery.

E. RF BREAKDOWN IN ARGON

A preliminary graph of breakdown voltage in argon is presented in Fig. X-4. This graph displays much the same features as the breakdown graph for hydrogen explained in a recent report.[10] The breakdown voltages are lower than for hydrogen and the oscillation amplitude limit is shifted to the left about half an order of magnitude. Further data will be taken to cover the range $10^{-6} < d/\lambda < 4 \times 10^{-2}$. These data are invaluable in TR tube design.

F. GASEOUS PULSED ATTENUATOR FOR MASER PROTECTION

There is a real need for a device which will give 100- to 130-db isolation for use in radars where masers are employed. Maser performance is quickly degraded by small amounts of leakage. In addition to high isolation in the transmit condition, the device must produce a minimum of insertion loss on receive or else the maser noise figure is impaired. A device which meets these requirements has been designed and the first model is being tested. It is made up of a long (12-inch) quartz tube of about 7 mm in diameter, placed along the axis of an X-band waveguide and filled with helium at low pressure (2 mm Hg).

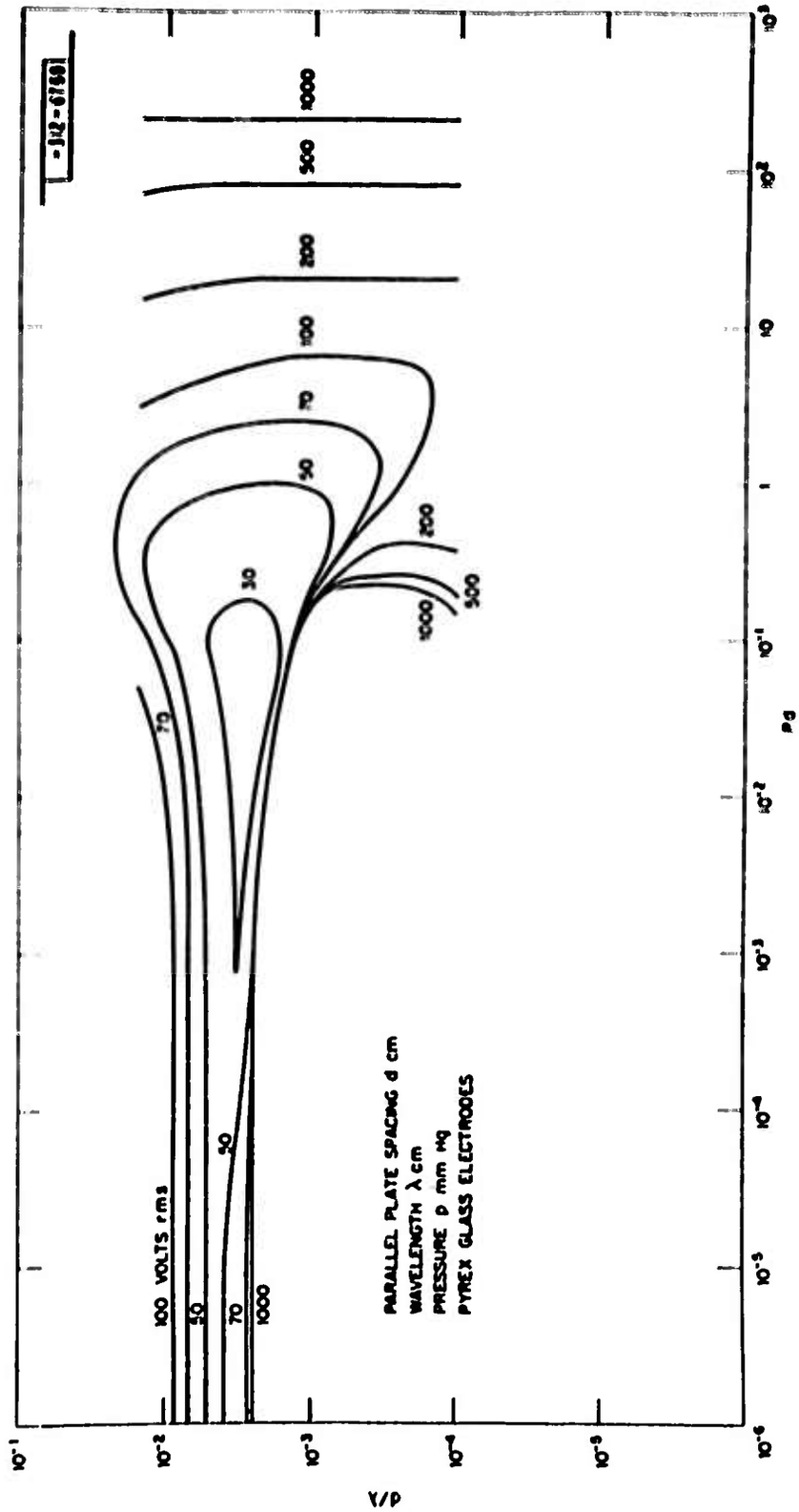

Fig. X-4. Contours of constant breakdown voltage for argon.

The tube has an oxide-coated cathode at one end and a simple anode at the other. A negative voltage pulse of about 2000 volts is applied to the cathode in series with a resistance sufficient to limit the current to about 250 ma. Attenuations in excess of 100 db have already been measured, the measurement being limited by the apparatus presently available. The insertion loss is calculated to be about 0.05 db, but has yet to be measured. Life of the pulsed attenuator will probably be determined by gas cleanup and is a subject which will require some attention.

C. W. Jones
C. E. Muehe
C. B. Nelson
A. A. L. Browne

REFERENCES

1. High-Power Tube Program Semiannual Technical Summary Report to ARPA [U], Lincoln Laboratory, M. I. T. (30 June 1961), p. 5, item (3), ASTIA 260544.
2. R. W. Olthius, "An Ultraclean Diode as an Emission Tester for Microwave Application," ASTM Special Publication No. 246 (1958).
3. E. A. Coomes, "The Pulsed Properties of Oxide Cathodes," J. Appl. Phys. 17, 647 (1946).
4. High-Power Tube Program Semiannual Technical Summary Report to ARPA for 30 June 1961, pp. 11-17.
5. D. MacNair, "Hydrogen Conversion of Thermionic Emitters Containing Alkaline-Earth Carbonate," Report on the Twenty-First Annual Conference on Physical Electronics (1961), p. 1.
6. High-Power Tube Program Semiannual Technical Summary Report to ARPA for 30 June 1961, p. 31.
7. M. Feinleib, Report on the Twenty-First Annual Conference on Physical Electronics (1961), p. 262.
8. L. A. Harris, Rev. Sci. Inst. 30, 831 (1959).
9. C. E. Muehe, "High Power Duplexers," Trans. IRE, PGMTT MTT-9, 506 (1961).
10. C. E. Muehe, "Some Aspects of High Power Window Design," G-Report 46G-0003 [U], Lincoln Laboratory, M. I. T. (3 October 1960), ASTIA 244326, II-172.